EuroSDR

European Spatial Data Research

April 2014

Change Detection in High-Resolution Land Use/Land Cover Geodatabases (at Object Level)

Emilio Domenech, Clément Mallet

A survey on state of the art of 3D Geographical Information Systems

Volker Walter

Dense Image Matching Final Report

Norbert Haala

Crowdsourcing in National Mapping

Peter Mooney, Jeremy Morley

Official Publication N° 64

Published by EuroSDR

printed by Buchdruckerei Ernst Becvar, Vienna, Austria

EUROPEAN SPATIAL DATA RESEARCH

PRESIDENT 2012 – 2014:

Thorben Brigsted Hansen, Denmark

VICE-PRESIDENT 2013 – 2017:

André Streilein-Hurni, Switzerland

SECRETARY-GENERAL:

Joep Crompvoets, Belgium

DELEGATES BY MEMBER COUNTRY:

Austria: Michael Franzen
Belgium: Ingrid Vanden Berghe; Jo Vanvalckenborgh
Croatia: Željko Hećimović; Ivan Landek
Cyprus: Andreas Sokratous, Georgia Papathoma
Denmark: Thorben Brigsted Hansen; Lars Bodum
Finland: Juha Hyyppä, Jurkka Tuokko
France: Benedicte Bucher, Yannick Boucher
Germany: Hansjörg Kutterer; Klement Aringer; Lars Bernard
Ireland: Andy McGill, Kevin Mooney
Italy: Fabio Crosilla, Alesandro Capra
Netherlands: Jantien Stoter; Martijn Rijsdijk
Norway: Jon Arne Trollvik; Ivar Maalen-Johansen
Spain: Antonio Arozarena, Emilio Domenech
Sweden: Mikael Lilje
Switzerland: Francois Golay; André Streilein-Hurni
United Kingdom: Malcolm Havercroft; Jeremy Morley

COMMISSION CHAIRPERSONS:

Sensors, Primary Data Acquisition and Georeferencing: Fabio Remondino, Italy
Image Analysis and Information Extraction: Norbert Pfeifer, Austria
Production Systems and Processes: Jon Arne Trollvik, Norway
Data Specifications: Jantien Stoter, The Netherlands
Network Services: Jeremy Morley, United Kingdom

OFFICE OF PUBLICATIONS:

Bundesamt für Eich- und Vermessungswesen
Publications Officer: Michael Franzen
Schiffamtsgasse 1-3
1020 Wien
Austria
Tel.: + 43 1 21110 5200
Fax: + 43 1 21110 5202

CONTACT DETAILS:

Web: www.eurosdr.net
President: president@eurosdr.net
Secretary-General: secretary@eurosdr.net
Secretariat: admin@eurosdr.net

EuroSDR Secretariat
Public Management Institute
K.U. Leuven
Faculty of Social Sciences
Parkstraat 45 Bus 3609
3000 Leuven
Belgium
Tel.: +32 16 323180

The official publications of EuroSDR are peer-reviewed.

CHANGE DETECTION IN HIGH-RESOLUTION LAND USE/LAND COVER GEODATABASES (AT OBJECT LEVEL)

Participants

Project Leader	**Emilio Domenech**	Instituto Geográfico Nacional (España)
Partners	**Clément Mallet**	Institut National de L'Information Geographique et Forestière
	Antonio Arozarena	Instituto Geográfico Nacional (España)
	Luis Ángel Ruiz Txomin Hermosilla Jorge Recio José Luis Gil	Universidad Politécnica de Valencia
	José A. Malpica María C. Alonso Alex Martínez Borja Rodríguez	Universidad de Alcalá
	María González Lourdes Albizua	Tracasa – Universidad Pública de Navarra
EuroSDR Chairman Commission 2	Norbert Pfeifer	Vienna University of Technology
Reviewers	Franzen Michael Nuria Valcárcel	Bundesamt fuer Eich-und Vermessungswesen – BEV Instituto Geográfico Nacional (España)

1. Introduction

The use of geospatial information is growing continuously. In order to satisfy this demand, geospatial databases must be frequently updated, with the highest possible metric and thematic accuracy. The main sources of updates are aerial or satellite images, which are complemented by other types of information, such as LiDAR (Light Detection And Ranging).

The most popular geospatial databases are those that provide land-use/land-cover information, since they provide key information for land management and environmental planning. These databases are internationally known as Land Use/Land Cover (LULC). Land use refers to the territory characterised according to its current and future planned functional dimension or socio-economic purpose, while land cover is an abstraction of the physical and biophysical cover on the earth‘s surface. Traditionally, LULC databases have been updated by means of photo-interpretation of aerial and satellite images, and by field visits. These techniques are lengthy, subjective, and costly. The utilization of digital techniques in the processing of aerial images reduces the volume of information that needs to be interpreted manually. It would be desirable to have automatic or semi-automatic methods offering the greatest possible degree of automation. LULC data are related to climatic and meteorological components, such as the interchange of gases for the greenhouse effect, and heat and radiation between the land surface and the atmosphere. Changes in LULC could affect ecosystems and, consequently the services and benefits that ecosystems provide to society.

The main objective of the present work is to study automatic image classification techniques applied to LULC geospatial information. These techniques allow the detection of changes, which are then used to update geospatial LULC databases.

Among the many different types of LULC, we focus on those that are similar to the Spanish SIOSE, but the proposed method would be valid for other LULC databases with scales close to 1:25,000. This could be considered a high-resolution LULC database, as the title of this EuroSDR project indicates. Furthermore, we focus on urban areas because this is where most major changes occur.

Geospatial data have been collected and changes have been studied for two dates, 2005 and 2010, for a case study of an urban area of Madrid, the city of Alcala de Henares. A second case study also analyzed an urban and periurban area of the city of Valencia, using data from 2004 and 2008. The last case study corresponds to a rural area from Murcia with data from 2007 and 2009. The Madrid study compares data from the SIOSE cartographic database for 2005 against imagery (aerial images and LiDAR data) from 2010; the Valencia case contrasts imagery (Quickbird and LiDAR data) between two years 2004 against imagery (aerial and LiDAR data) for 2008; in the Murcia study is compared a LU/LC database from 2007 with aerial orthoimages of 2009. This approach permits the proposed method to be tested for different data, different survey dates, and different places.

The proposed method is the same for the study areas; it is an object-oriented approach, based on rules used by Dempster–Shafer theory (DS theory), following satisfactory results previously obtained using this theory with per-pixel methods (Mena and Malpica, 2005; Malpica et al.,

2012). In the present study, Dempster–Shafer theory has been extended with an object-oriented perspective, using a Region Adjacency Graph (RAG).

Aerial and high-resolution satellite images provide a huge amount of detail, and are very useful for cartographic works; however, high resolution also introduces problems of shadows, which entail a devaluation of the radiometry for certain areas of the images. This problem is tackled here using the LiDAR data and metadata of the image.

The main idea for LULC change detection is to achieve reliable classification of the imagery. To do this, since classes are related to each another, it is necessary to assign classes to every pixel or region in the image. A human operator examining an aerial image knows that a road is not interrupted by a group of high trees; that the road may be obscured beneath the tree canopy, and continues beyond them; or that a shadow region close to a large lawn should also be categorized as a lawn. In order to successfully employ automatic classification, it is necessary to employ sufficiently flexible rules to somewhat emulate the knowledge of the human operator, and to allow the system some means of "reasoning," an approach that is known in other fields as an "expert system." A first step in this direction could be a system of rules (knowledge) and Dempster–Shafer theory (reasoning). We have applied this approach in the present work, and found it useful to define a RAG for the regions, providing topological information to the system. This remains a work in progress, but the results already obtained indicate that it could be used for interactive work when determining LULC change detection. Much work remains in order to obtain a completely automated system of LULC change detection; this should be a long-term objective but, meanwhile, we should concentrate on developing a semi-automatic (interactive) system that could help in the manual photointerpretation of LULC geospatial databases. This forms the objective of the present work, without losing the objective of developing as fully-automated a system as possible.

2. Objectives

To study and evaluate automated object-oriented image classification techniques applied to LULC databases

To integrate high-resolution images, airborne laser scanner data, and database information to improve the efficiency of the methods

To assess the use of these techniques for thematic geospatial database updating and change detection

3. Study areas and data pre-processing

In this chapter, the study areas and the main characteristics of the data used in the project are described.

Table 1 summarizes the data used from the different study areas.

Table 1. Available data from the study areas.

Zone	Data
Alcalá	LiDAR PNOA 2010 – 0.5 point/m^2
	DTM 2006 – stereo matching
	Orthoimages RGB PNOA 2006. IR 2009
	Corine 1990, 2000, 2006
	SIOSE
Valencia north	LiDAR 2004 -1 point/m^2
	LiDAR PNOA 2009
	ORTOS IR PNOA 2006, 2008
	SIOSE
	QuickBird 2004 RGB+IR+PAN
Murcia	LiDAR PNOA 2009 – 0.5 point/m^2
	DTM 2004, 2007 – stereo matching
	Orthoimages IR PNOA 2007, 2009.
	Corine 1990, 2000, 2006
	SIOSE

(a) (b) (c)

Figure 1. Detail of 4-band image (B, G, R, and NIR) of Alcalá (a), Valencia periurban area (b), and detail of a 3-band image (IR, R, G) of Murcia with parcels overimposed(c).

3.1. Alcalá de Henares data

This study area is an example of an urban area with several urban typologies from historical to industrial. Two types of data are available for Alcalá de Henares: high-resolution aerial imagery, and LiDAR data. This data were collected by the Spanish National Mapping Agency (NMA), as explained in Arozarena and Villa (2005). Usually, aerial imagery is acquired for the whole of Spain every two years, and LiDAR data is collected within the PNOA (Plan Nacional de Otofotografía Aérea) program. An example of an aerial image from PNOA can be seen in Figure 1.a, showing an urban area of Alcala de Henares city. This image has 4 colour bands (blue, green, red, and near-infrared), and was acquired in 2010 with a spatial resolution of 0.5 m.

Although the acquisition resolution was of 0.5 m, the image was resampled to a resolution of 1 square meter, in order to combine the information of the original image with the LiDAR data that was resampled to this resolution, as explained next.

The LiDAR data was used to produce a Digital Surface Model (DSM). The DSM was used to produce a Digital Terrain Model (DTM) (Martinez de Agirre and Malpica, 2010); then, subtracting these two, a normalized DSM (nDSM) model was obtained. PNOA images as well as the nDSM were geo- referenced, and a co-register was taken of both to a resolution of 1 meter.

3.2. Valencia data

This area can be differentiated in two main areas: urban and suburban. Urban areas correspond to the centre of the city, with historical, urban planned, isolated buildings, etc. The suburban area (Figure 1.b) correspond to the northern part of Valencia, composed of a mix of rural (mainly agricultural parcels) and urban periphery buildings (including detached and semi-detached houses, industrial, etc.).

The area of Valencia has approximately 5,372 ha, and it has undergone important changes in LU/LC for the last decade, including the transformation and urbanization of large agricultural areas formerly covered by orchards and horticulture crops, and the removal of some industrial and agricultural structures. The objects for the analysis were defined using the plot boundaries derived from cadastral maps produced by the Spanish General Directorate for Cadastre (Dirección General de Catastro), with a scale of 1:1,000 in urban areas and 1:2,000 in rural areas. (Urbana y peri-urbana)

High-resolution multispectral imagery and LiDAR data were available for both epochs. For the first epoch, QuickBird imagery acquired in February 2004 was available, with 11 bits/pixel radiometric resolution and four spectral bands (visible and near infrared). The multispectral and panchromatic bands were merged using the substitution method based on principal components transformation, obtaining a final spatial resolution of 0.6 m/pixel. The image was georeferenced

and orthorectified. LiDAR data were acquired in December 2003 by an ALTM-2033 sensor, and a digital surface model (DSM) having a grid size of 1 m was computed. In addition, a manually edited digital terrain model (DTM) was available. The normalized digital surface model (nDSM) was generated as the difference between the DSM and the DTM.

Additional aerial images were acquired in August 2008 in the framework of the Spanish National Plan of Aerial Orthophotography (PNOA), with 0.5 m/pixel spatial resolution, 8 bits/pixel radiometric resolution and four spectral bands in the visible and near infrared domains. These images were orthorectified and georeferenced. Panchromatic and multi-spectral bands were merged, and mosaicking and radiometric adjustments were applied as a part of the PNOA programme. LiDAR data were acquired in September 2009 using a RIEGL LMS-Q680 sensor with a nominal density of 0.5 points/m2. The DTM (Figure 2.c) was computed by means of the iterative algorithm described by Estornell et al. (2011) that selects minimum elevation points and eliminates points belonging to above-ground elements such as vegetation or buildings. DSM (Figure 2.d) was computed using original LiDAR point cloud (Figure 2.a). nDSM (Figure 2.d) was calculated by the subtraction of the DTM from the DSM.

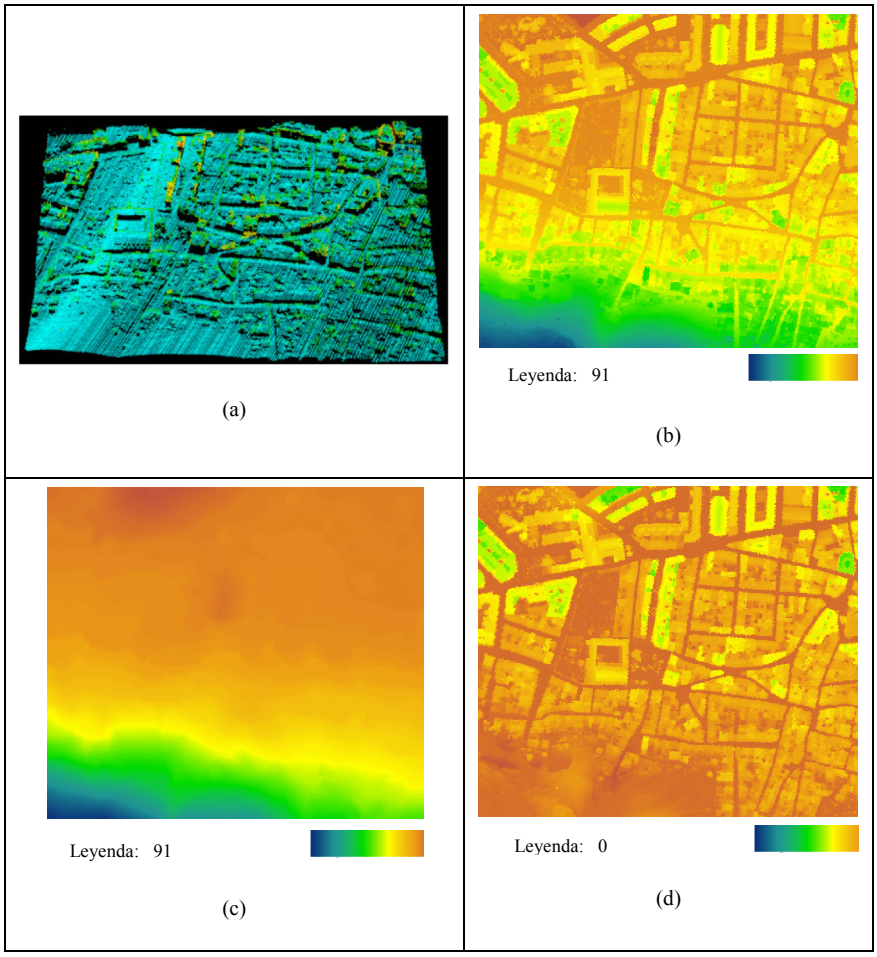

Figure 2. (a) LiDAR data point cloud, (b) DSM, (c) DTM y (d) nDSM.

3.3. Murcia data

The study area of Murcia (Figure 1.c) corresponds to a rural area with crops, orchards, irrigation ponds, etc. In this area, changes are related to crops removal, new crops and creation of irrigation ponds. In this area, an official database provided by the CARM (Comunidad Autónoma de la Región de Murcia), where cadastral parcels are defined, was used to define the objects for the analysis.

Aerial images from the PNOA are available for 2007 and 2009, with 0.5 m/pixel spatial resolution, 8 bits/pixel radiometric resolution and four spectral bands in the visible and near infrared domains. Images were orthorectified and georeferenced, mosaicking and radiometric adjustments were applied as part of the PNOA programme.

LiDAR 2009 data was also acquired from the PNOA programme, with a nominal density of 0.5 points/m^2, acquired by a RIEGL LMS-Q680 sensor. DTM was obtained using similar methods and algorithms that those used in Valencia area.

4. Methodology

The proposed methodology combines high resolution imagery, LiDAR data and database polygons as input data, generating two types of outputs: basic land cover classes, and land use related to the objects. In our tests, the objects are delineated using the cadastral database polygons, but any other type of polygon could be used. The legend is defined following the guidelines of the SIOSE database.

The process can be divided into two main phases:

- Segmentation and classification in basic land cover (LC) classes based on Dempster-Shafer theory.
- Classification in land use (LU) of objects based on multi-source descriptive attribute extraction and decision trees.

These two main procedures are described and tested separately. Then, a change detection approach is proposed based on the integration of both. The main flowchart is shown in Figure 3.

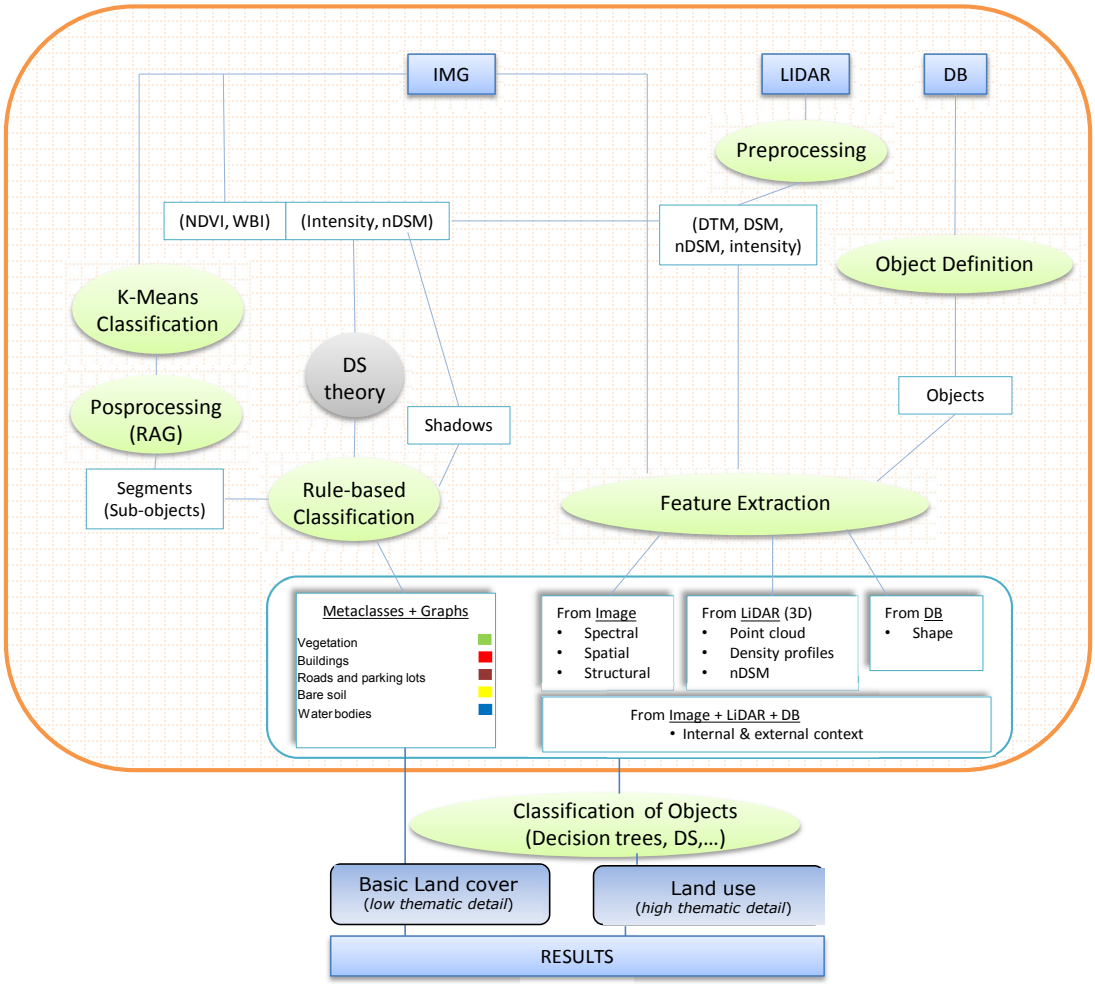

Figure 3. Overall flowchart for change detection.

4.1. Classification in basic land cover

The objective of this phase is to generate basic LC classes of the objects obtained from segmentation. This phase can be divided in 4 different steps:

- Image segmentation
- Region Adjacency Graph (RAG)
- Classification improvement using Dempster-Shafer theory
- Shadow removal

In Figure 4 the workflow of this phase is shown.

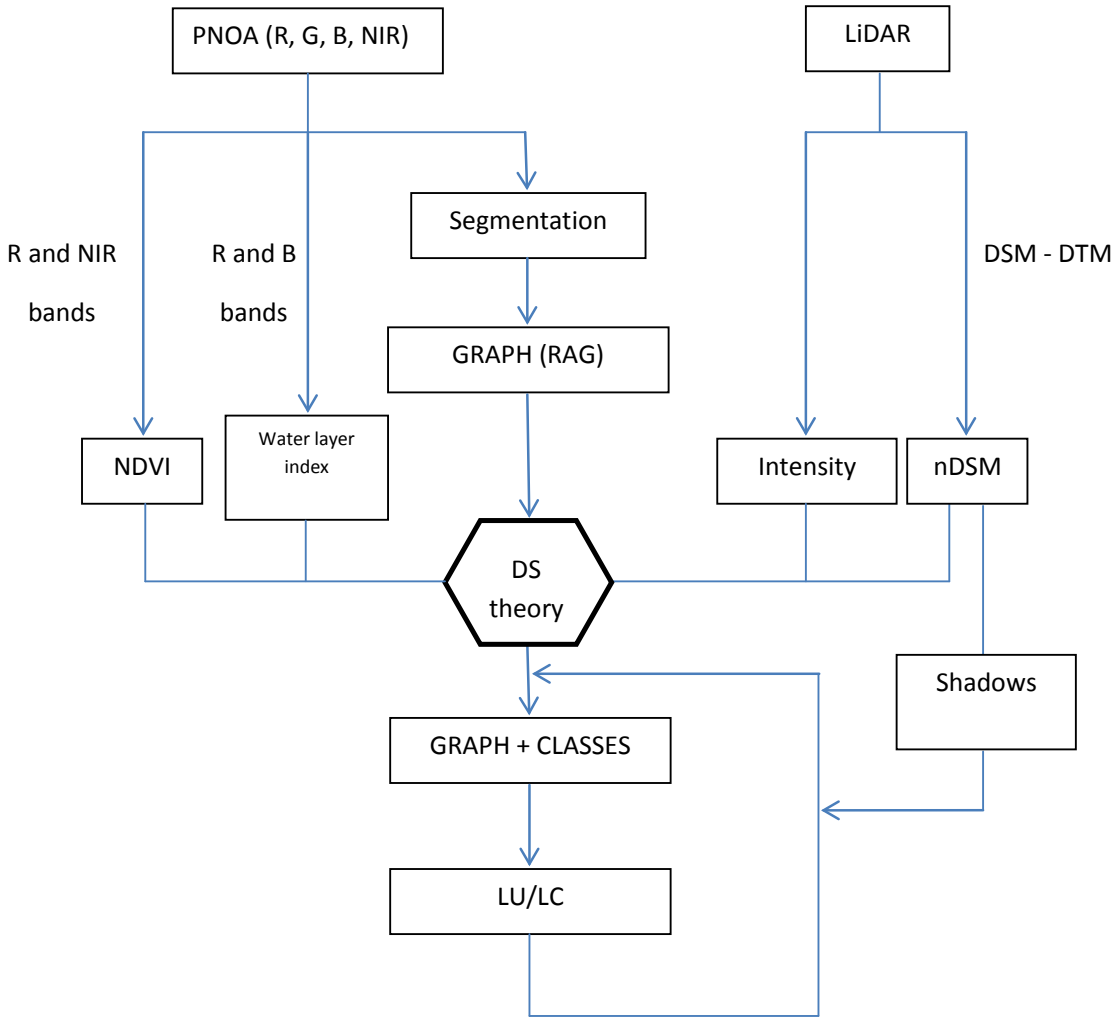

Figure 4. Basic land-cover classification flowchart.

4.1.1. Image segmentation

Usually, the first step in the process of obtaining information from an aerial image to produce a land-cover layer is to perform data segmentation. The purpose of segmentation is to simplify the representation of an image in a way that is more meaningful and easier to analyze, trying to work at a region level rather than at pixel level, as animal vision does: rather than individual pixels, the brain of an animal "sees" homogenous regions that the brain is able to interpret in a subsequent process. There are many image segmentation methods, including clustering (Wu and Leahy, 1993), thresholding (Haralick and Shapiro, 1985), and region growing (Bins et al., 1996).

Fuzzy K-means (FK-means, also known as Fuzzy C-means) is an extension of the popular K-means unsupervised classification method. While K-means identifies hard clusters (a point belongs to only one cluster), FK-means identifies soft clusters, where a particular point can belong to more than one cluster with a given probability. Therefore, FK-means is a more

statistically formalized method than K-means. The disadvantage is that it is more processor-intensive, since it has to perform a larger number of operations.

Although FK-means is not a proper segmentation method, we used this unsupervised classification technique to decompose the image into homogenous regions. The whole purpose of classification is to partition a set of objects into classes or categories; these classes are constructed so that a pixel in a given group is similar in some sense to those neighbouring it, to any other pixel belonging to the same group or class. The similarity between observations is stated in terms of the spectral distances between pixels. In the case of the FK-means classification used here, the only parameter determined by the user is the number of classes (Duda and Canty, 2002; Canty and Nielsen 2006). Unlike the process of region-growing segmentation, in which it is necessary to introduce two parameters—the seed points and a threshold—in an unsupervised classification algorithm such as FK-means, it is necessary to specify only the number of classes by which to classify the image; the higher the number of classes, the greater the number of regions to be generated in the segmentation. Since no more information is necessary from the user, the FK-means is an unsupervised classification.

After the classification has been performed, the groups were labelled, which served to move them from class to regions, i.e., from a classification process to a segmentation process. This operation gave each region a unique identifier (Rodriguez-Cuenca et al., 2012).

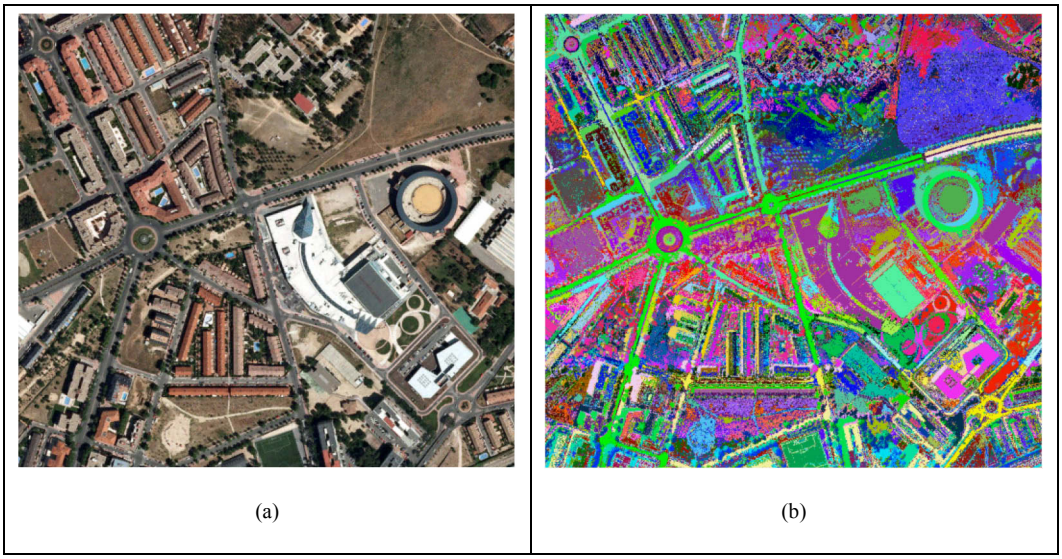

(a) (b)

Figure 5. (a) aerial image; (b) result of applying FK-means segmentation.

Figure 5 shows the result of applying FK-means classification. This classification takes into account only the spectral characteristics of the image; however, with the addition of labelling and post-processing, it is converted in a real segmentation process.

4.1.2. Region adjacency graph

A graph is an abstract structure composed of vertexes and edges. Once the image is segmented into regions, a Region Adjacency Graph (RAG) is considered. Each region is associated with a node or vertex of the graph, and then edges are created between every pair of vertexes that represent neighbouring regions in the image.

Each node of the graph introduces all the necessary information, such as number of pixels, barycentre, median of the spectral value for a band, median of the NDVI index, etc.

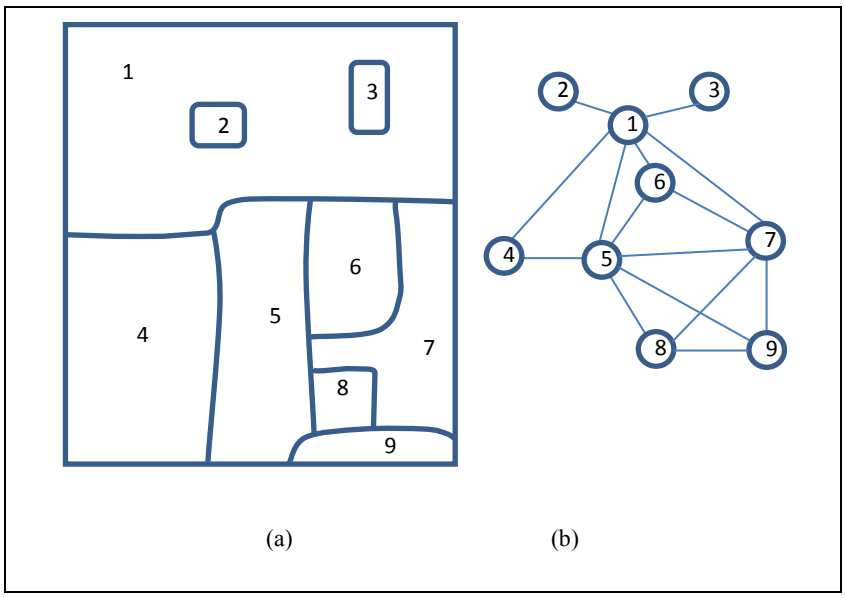

Figure 6. (a) an image segmented with 9 regions and (b) its corresponding RAG.

The RAG is applied to the segmented image using FK-mean to obtain an improved classification, merging regions that are probably of the same class (Jain et al., 1995). Figure 6 shows an image with 9 regions and its corresponding RAG.

The algorithm used to generate the RAG was the following:

1. Scan the membership over the image and perform the following steps at each pixel index [i,j]
2. Let r1 = a[i,j]
3. Visit each neighbor [k,l] of the pixel [i,j]. For each neighbor, perform the following task
4. Let r2 = a[k,l]. If r1 ≠ r2, then add an edge between nodes r1 and r2

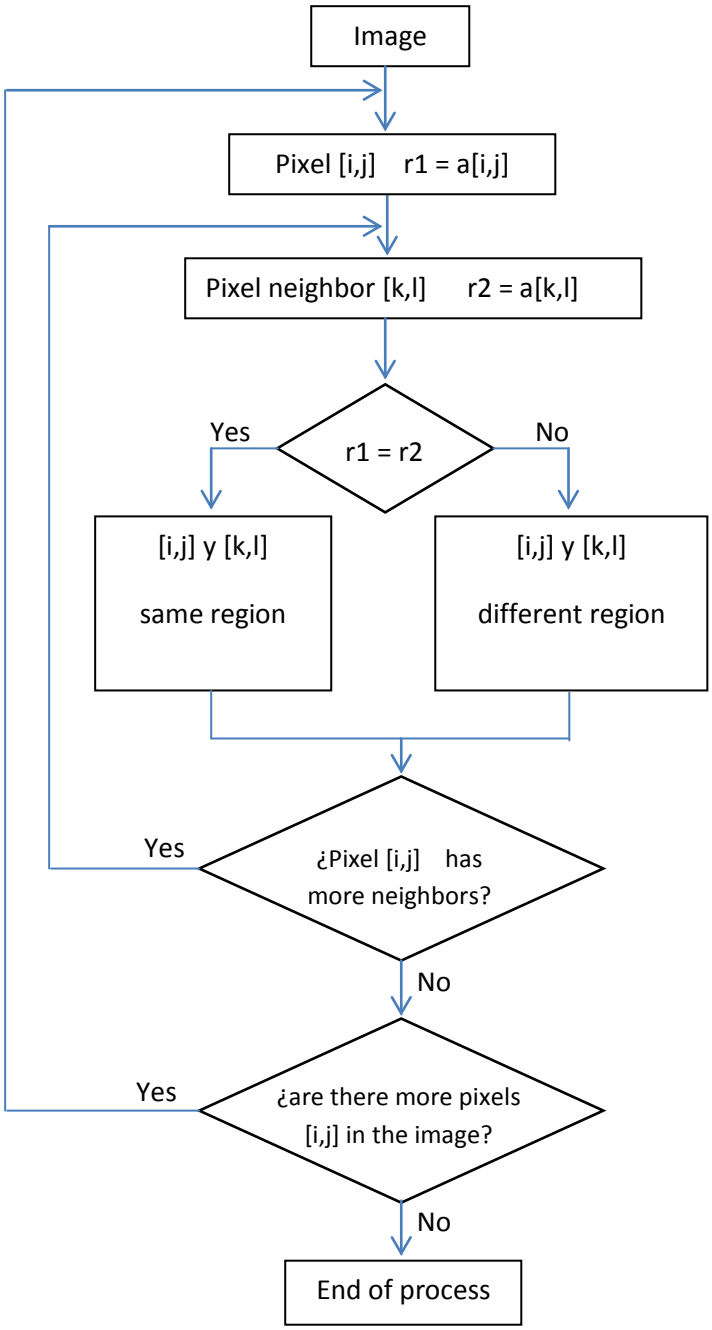

4.1.3. Image classification improvement using Dempster-Shafer theory

The Dempster–Shafer theory was first put forward by Dempster (1968) and later expanded by Shafer (1976), and sometimes it is called the theory of evidence. Its development was motivated by the difficulty of representing uncertainty within probability theory. The application of Dempster–Shafer to geoscience has been reported several times (e.g., Malpica et al., 2007)

The theory of fuzzy sets is a generalization of classical set theory. In classical set theory, an element does or does not belong to a set, whereas in fuzzy sets it can be said that an element has a degree of belonging to one or more sets. This degree is expressed by the following membership function:

$$A:\Omega\rightarrow[0,1] \tag{1}$$

where A(x) denotes the degree to which x belongs to A for each x $\in\Omega$, where Ω is in the classical set theory, the universal set. In Dempster–Shafer theory, it is called the frame of discernment.

If the cardinality of Ω is h, there are 2h subsets of Ω. These are called propositions, and they are the elements of $\wp(\Omega)$, which is the set of subset of Ω, also called the power set of Ω. As one can see, the development of fuzzy set theory and its notations are similar to those of classical set theory.

Given the frame of discernment Ω and a family not empty of subset C of Ω (with a suitable algebraic structure), a fuzzy measurement g in (Ω, C) is given by the following function:

$$A:C\rightarrow[0,1] \tag{2}$$

that verifies the following constraints:

[1] Boundary condition: g(C) = 0 and g(Ω) = 1

[2] A $\subseteq$ B then g(A) ≤ g(B)

We will not digress further into fuzzy measurement; instead, the reader can consult the book by Klir and Wierman (1999) for further detail. This measurement is the basis of three theories: Probability theory, Possibility theory, and Dempster–Shafer theory. Since we are considering only the fusion of information, we will reduce our attention to the latter Dempster–Shafer theory, which we will briefly introduce next. A fuzzy measurement is said to be a belief measurement β if the following is verified:

$$\beta:\wp(\Omega)\rightarrow[0,1] \tag{3}$$

β must verify

[1] $\beta(\phi)=0,\quad \beta(\Omega)=1$

[2] $$\beta\left(A_1\cup A_2\cup\cdots\cup A_n\right)\geq\sum_j\beta\left(A_j\right)-\sum_{j<k}\beta\left(A_j\cap A_k\right)+\left(-1\right)^{n+1}\beta\left(A_1\cap A_2\cap\cdots\cap A_n\right)$$

Associated with all belief measurement is a plausibility measurement ζ, which is also a fuzzy measurement, and is defined by the equation:

$$\zeta(A) = 1 - \beta(\bar{A}) \tag{5}$$

In Dempster–Shafer theory, a function is defined to characterize the measurements of belief and plausibility. This function is called the mass function, as follows:

$$\mu : \wp(\Omega) \rightarrow [0,1] \tag{6}$$

Such that $\mu(\phi) = 0$ and $\sum_{A \in \wp(\Omega)} \mu(A) = 1$. This mass function is determined in a unique way by the equations:

$$\beta(A) = \sum_{B \mid (B \subseteq A)} \mu(B) \tag{7}$$

$$\zeta(A) = \sum_{B \mid (B \cap A \neq \phi)} \mu(B) \tag{8}$$

The value of certainty has an inferior boundary, given by the plausibility, and a superior boundary, given by the belief. Plausibility and belief are analogous to optimistic and pessimistic measurements of certainty, respectively.

When there are several sources for studying a phenomenon, in the case when a class has to been a assign to a region using several sources (since there are several sources, such as NDVI, LiDAR intensity, Geometry indexes, etc.), then the Dempster–Shafer theory becomes useful. Hermosilla et al. (2012a and 2012b) studied several of these features, and they have been studied to be introduced as rule to the Dempster–Shafer theory. So far it has only been introduced in its simple form. The basic mass function for each source is denoted by μ(i), where i=1,…,n are the sources. If the sources are assumed to be independent, then the orthogonal sum of the Dempster–Shafer theory can be applied, which will allow the fusion of information. The orthogonal sum is defined by the equation:

$$\left(\mu_i \oplus \mu_j\right)(A) = \frac{\sum_{B \cap C \neq A} \mu_i(B)\mu_j(C)}{\sum_{B \cap C \neq \phi} \mu_i(B)\mu_j(C)}, \quad A, B, C \in \Omega \tag{9}$$

Kohlas and Monney (1995) described the formalization of the mathematical theory behind Dempster–Shafer theory. It is interesting to note that the orthogonal sum of Equation (9) is associative and commutative, which means that the sources could be mixed two by two, and the order is not important. Figure 7 shows the flow followed for entity extraction.

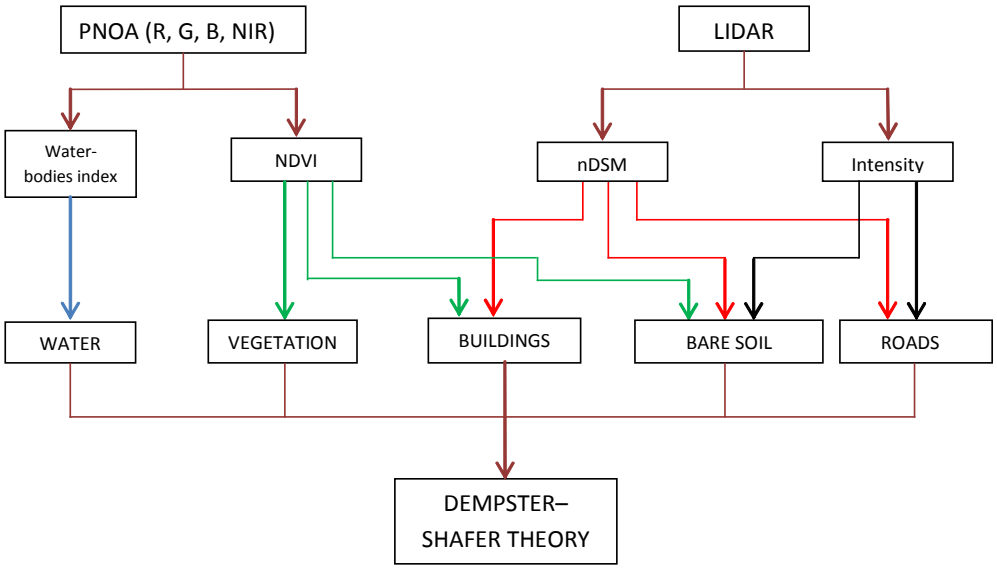

Figure 7. Diagram for entity extraction.

Of the various scenarios within urban areas, the LC classification in this study utilized five basic classes that follow the Spanish high-resolution LULC classification, SIOSE. These classes (shown in Figure 8) comprise urban vegetation, buildings, communications (roads and parking lots), bare soil, and water bodies.

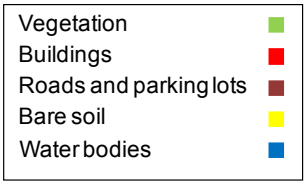

Figure 8. LC classes legend.

4.1.4. Shadow removal

4.1.4.1. Computing the shadow layer

The detection of shadows is a common problem in the analysis of aerial or high-resolution satellite imagery. The main problem caused by shadows is the reduction or total loss of information in some areas of an image. The loss of information could lead to corruption of biophysical parameters derived from the pixel values, such as vegetation index (Leblon et al., 1996). The effects of shadows are aggravated when abrupt changes in surface elevation occur, such as in urban areas, since buildings cast shadows that obscure information about other surface features in their surroundings.

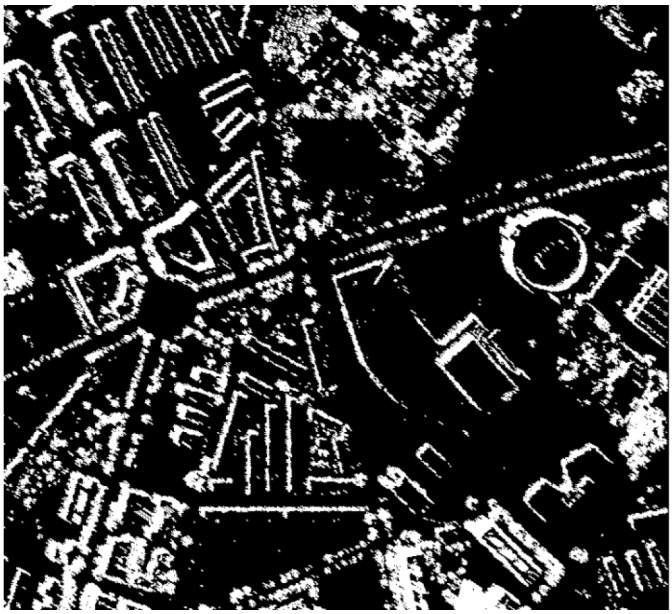

Figure 9. Binary image with shadows detected using the nDSM and metadata from the LiDAR data

The detection of shadows is achieved using the nDSM and the LiDAR metadata, such as the sun height at the time of the image acquisition (Martínez de Agirre and Malpica, 2012). (Example in Figure 9).

4.1.4.2. Assigning classes to shadow regions

The shading of an area can lead to incorrect classification or mapping for this type of coverage, due to the influence of the shadow in the spectral response. It has been observed that, in some cases, shadow regions caused false-positives in the NDVI, and in ad hoc indexing created to detect water bodies. Generally, bare ground, a road, or urban vegetation is classified as water when it is in shadow. Figure 10 shows a detail where this type of error occurred.

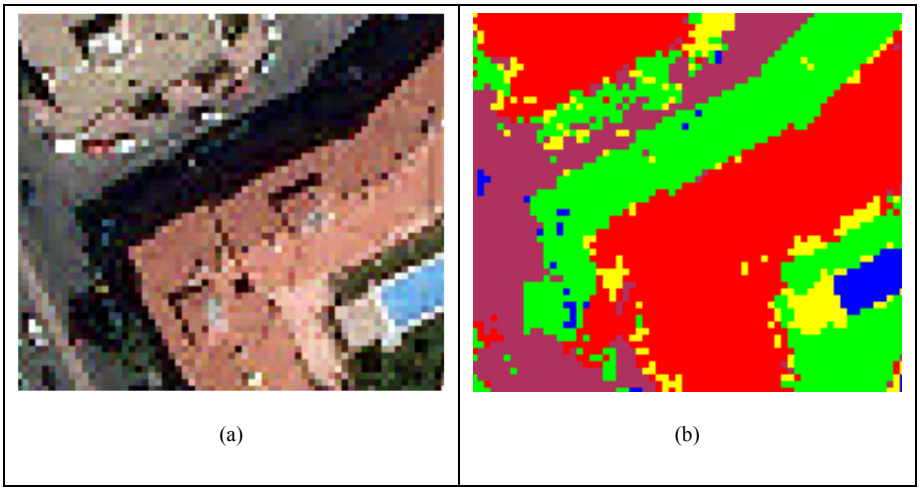

Figure 10. (a) detail of aerial image with a shadow region close to a building; and (b) LULC classification with errors for shadow regions. In this case the shadow region has been classified as vegetation.

In order to refine the initial segmentation by FK-means, a clean-up was performed of those regions classified as water bodies that had a high probability of being shadows. The algorithm examined all the nodes, and used Dempster–Shafer theory to detect those regions with high probability of being shadows and water bodies, and these were assigned to the larger neighboring region. As it can be seen in this case, the classification was conducted not according to the spectral properties but to the spatial properties, because when a region is in shadow the spectral properties vary considerably. Thanks to the graph structure, it is possible to introduce a more intelligent form of classification to the process. So far, the rules employed have been very simple, but the improvement is very satisfactory, which demonstrates the potential of the proposed method.

Figure 11 shows a detail of how to clean a shadow region labelled as a water body. Figure 11.a shows an aerial image corresponding to Alcala's bullring and its surroundings; Figure 11.b shows the classification using Dempster–Shafer theory over the FK-means segmentation. It can be observed how the seating in shadow has been incorrectly classified as a water body, which would be impossible in this context. Figure 11.c shows the shadow layer, and Figure 11.d shows how the error has been resolved by reclassification through Dempster–Shafer theory; the region initially classified as a water body is automatically reclassified as a building, since this is the class assigned to the larger neighbouring region.

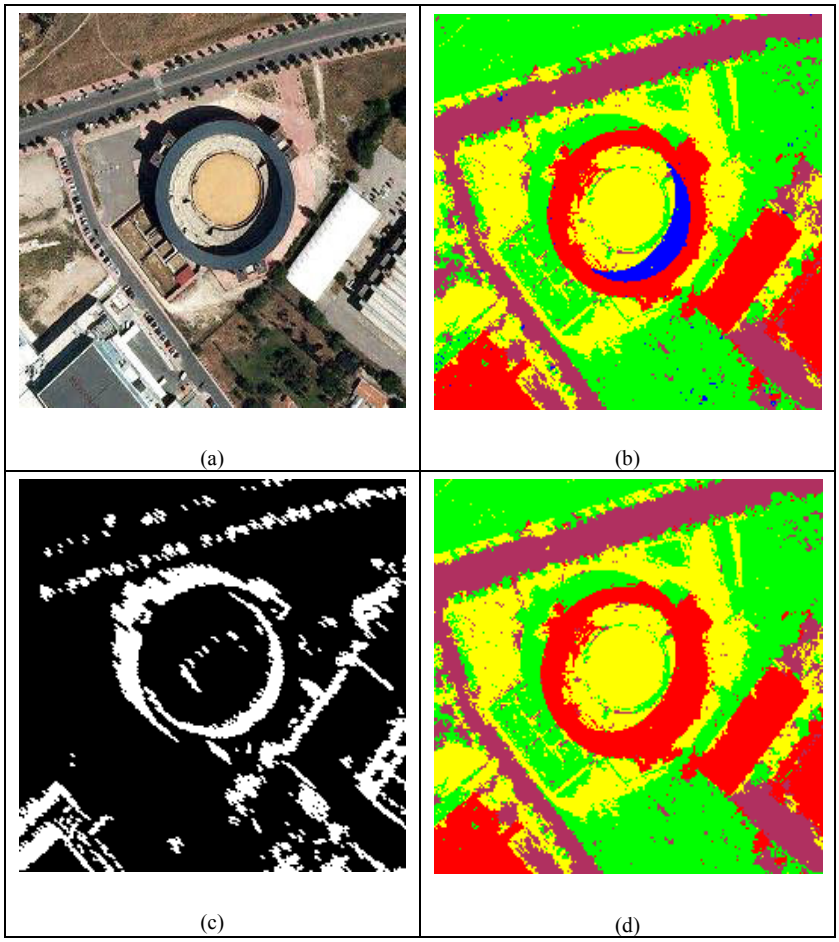

Figure 11. (a) Detail of the aerial image showing Alcala's bull fighting arena and surroundings; (b) Initial classification of LULC with the Dempster–Shafer theory; (c) Shadow layer computed from the nDSM and metadata; and (d) Second application of Dempster–Shafer theory, using the RAG, assigning shadow regions to other classes when necessary.

4.2. Multi-source attribute extraction and land use classification

This phase (Figure 12) is based on the definition of objects from a database (cadastral plots, SIOSE polygons, etc.), the extraction of an exhaustive set of descriptors from images, LiDAR and the database and the classification of the objects in different land uses. It can be divided in two steps: feature extraction and object-based classification.

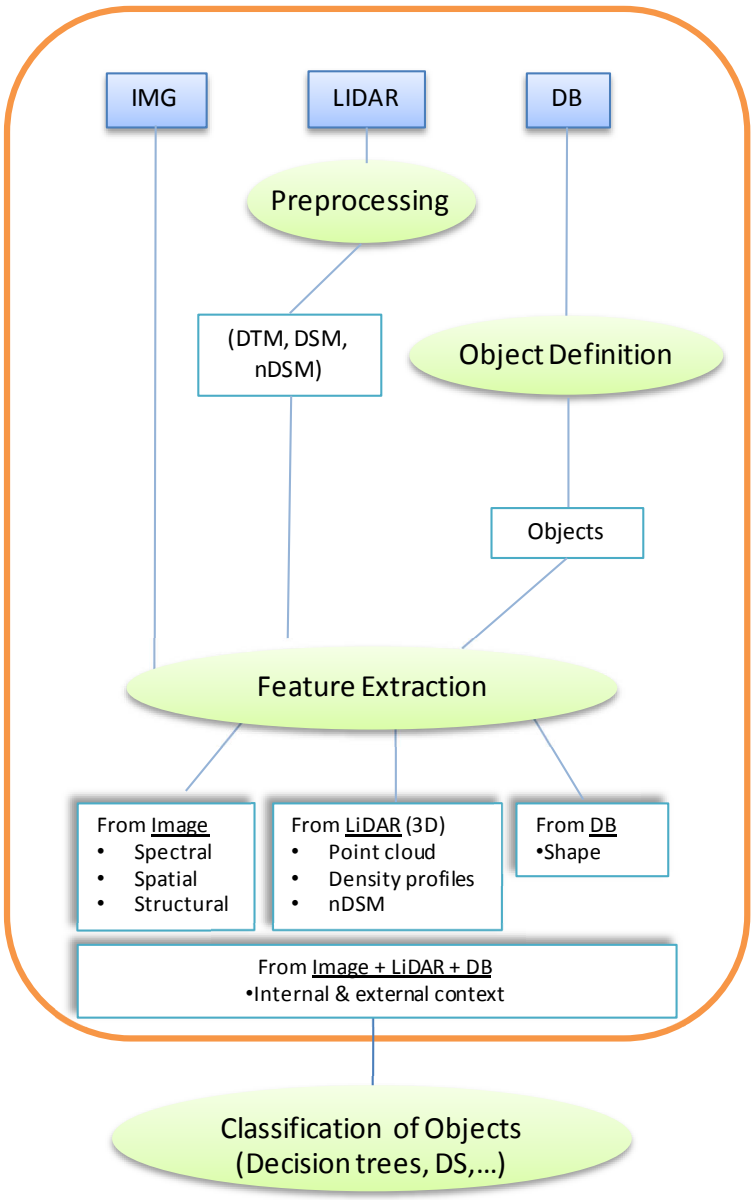

Figure 12. Land use classification flowchart.

4.2.1. Feature extraction

Descriptive features were extracted from objects (both, segmented and cadastral polygons) attending to three different object aggregation levels: object-based, related to internal context and related to external context (see Figure 13), as reported by Hermosilla et al. (2012a). Object-based features describe the properties of each object (plot) considered as a single unit. They were computed using the object-based feature extraction software FETEX 2.0 (Ruiz et al., 2011). These descriptive features provide information about spectral, textural, geometrical, and 3D properties. Spectral features inform, through the intensity values of the pixels contained in the plots, about the objects' overall spectral behaviour in the different spectral bands used.

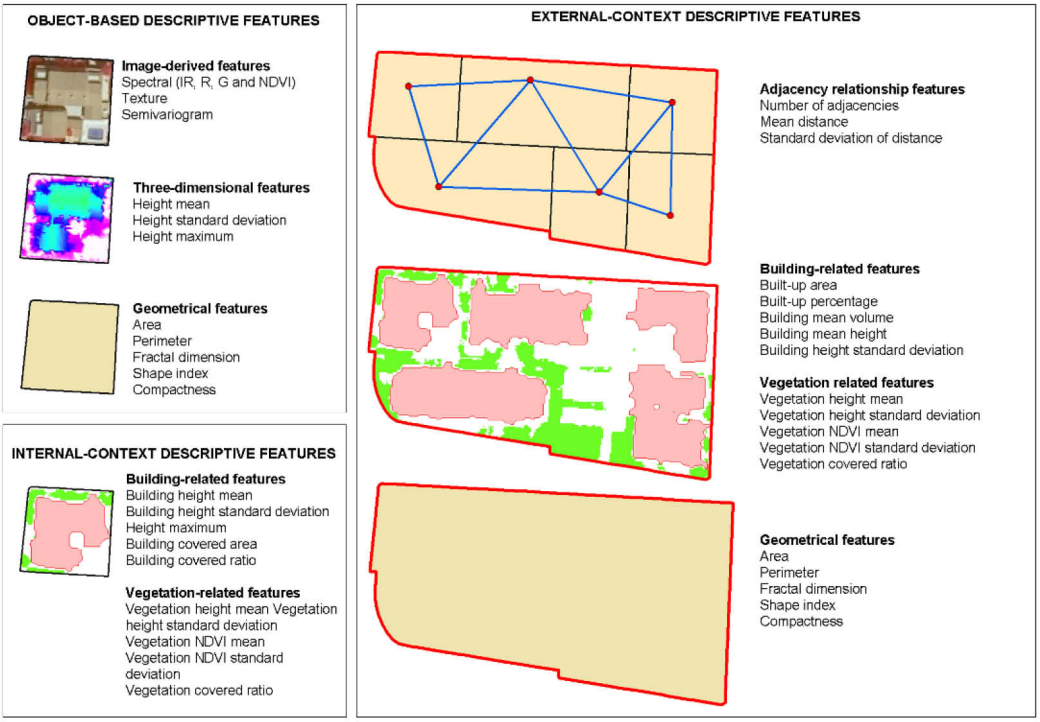

Figure 13. List of features computed and graphic examples.

Mean standard deviation, as well as minimum and maximum of the intensity values of the pixels for all available bands, and normalized difference vegetation index (NDVI) and water body index (WBI) images were computed for each object.

Figure 14.a shows the NDVI image where can be observed (details b and c) how regions with vegetation in the aerial image are represented by high levels of gray colour in the digital NDVI image.

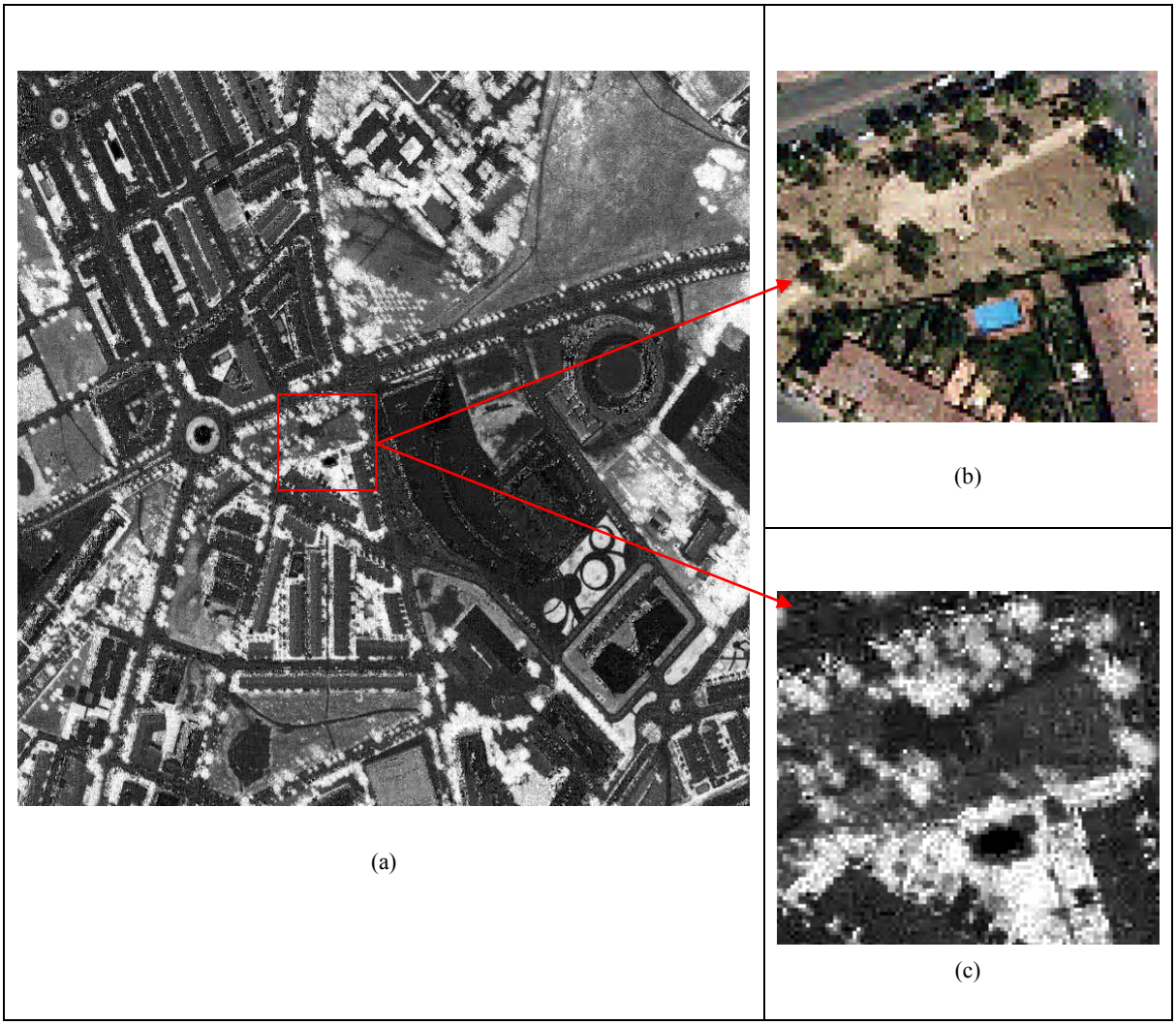

(a)

(b)

(c)

Figure 14. (a) NDVI image obtained with equation (1); (b) detail of RGB area with vigorous vegetation; (c) corresponding area in the NDVI image.

Water bodies have a distinctive spectral signature, since they reflect very little of the electromagnetic spectrum, with only a small peak in the blue band (if this is the colour of the water in the image). A similar index to the NDVI was computed using the red and blue bands:

$$WBI = \frac{B - R}{B + R} \tag{10}$$

where WBI represents Water Body Index, and B and R are the blue and red bands, respectively. This index produces a high value for water bodies but also false-positives in shadow regions. Figure 15 shows a detail of the image after applying the water body index. As can be seen, swimming pools are assigned higher values.

Figure 15. Layer produced with the Water Body Index

4.2.1.1. LiDAR-based features

The LiDAR data not only provides the DSM and DTM, but also intensity information. Low LiDAR intensity values are obtained in asphalt areas. This was used to detect roads and parking lots in the image. As certain buildings have asphalt roofs, the model incorporates the Dempster–Shafer theory rule of intensity of LiDAR data with that from the nDSM, so only regions that have a low intensity value combined with a low elevation would be classified as roads or parking lots. Figure 3.8 shows the layer for the LiDAR intensity, where roads, parking lots and some buildings (presumably with an asphalt roof) are distinguished.

Texture features quantify the spatial distribution of the intensity values in the analyzed objects. The following descriptive features were derived: histogram kurtosis and skewness; descriptors derived from the grey level co-occurrence matrix (GLCM) and proposed by Haralick et al. (1973); edgeness factor (Sutton & Hall, 1972); and semivariogram-based descriptive features (Balaguer et al., 2010). Three-dimensional features were derived from the nDSM computed from LiDAR data, each object being characterized by the mean, standard deviation and maximum values of the heights. Geometrical features describing the dimensions of the objects and their contour complexity were computed: area, perimeter, compactness (Bogaert et al., 2000), shape index and fractal dimension (Krummel et al., 1987; McGarigal & Marks, 1995).

Some of the context-based features were based on the area covered by buildings and vegetation inside each object, since this distribution is strongly related to the different urban typologies. Building and vegetation masks were obtained as a result of the LC segmentation/classification in basic classes. Buildings and vegetation correspond to the sub-objects inside the plots.

Internal-context features describe an object by characterizing the internal sub-objects of the plots. Both 2D and 3D features describing the buildings inside each object were computed. The 2D features consist of the built-up area and the percentage of built-up areas in an object. The

latter feature – usually referred to as building coverage ratio (BCR) or sealed surface (Yoshida and Omae, 2005; Van de Voorde et al., 2009; Yu et al., 2010) – is computed as:

$$BCR = \frac{A_{Building}}{A_{Object}} \cdot 100 \qquad (11)$$

where $A_{Building}$ is the built-up area, and A_{Object} is the area of the considered object. Buildings were also characterized by a set of 3D features describing their heights, using the mean, standard deviation, and maximum values from the nDSM. Similarly to (eq. 11), the percent-age of surface covered by vegetation within an object was defined, and additionally a set of statistical descriptors of height and status of vegetation sub-objects (mean and standard deviation of nDSM and NDVI, which were computed solely from groups of vegetation pixel) was computed.

4.2.1.2. Spatial context features

External context is described by considering the spatial relations of adjacent objects by means of building-based, vegetation-based, geometrical and adjacency features. Adjacency between objects was characterized based on the graph theory (Laurini and Thomson, 1992) by using the number of neighbours with surrounding objects, as well as the mean and standard deviations of the centroid distances between adjacent objects. The shape, size, and number of buildings per block are often related to their socio-economic function and determine the area and volume for an urban block. Therefore, the land use of an urban block may be indicated by the quantitative observations related to the buildings present in it (Yoshida and Omae, 2005). Thus, urban blocks were also characterized by the built-up area and the built-up percentage. The height distribution of the buildings contained in an urban block was described using the height mean and standard deviation values obtained from the nDSM. Features related to the volumetric information of buildings were also considered. Thus, the mean volume was computed as the total volume of buildings divided by the number of buildings contained in the block. In a similar manner to the internal context features, vegetation distribution was characterized using the vegetation cover ratio, as well as the mean and standard deviation values of the nDSM and NDVI obtained only from the vegetation area masked within the super-object. Finally, the geometrical properties of the urban blocks were described using the features area, perimeter, compactness, shape index, and fractal dimension.

4.2.2. Object classification

4.2.2.1. Object and class definition

The basic unity employed has been defined combining rural cadastral sub-parcels and urban cadastral parcels. Rural sub-parcels are the internal divisions on the cadastral parcels as a consequence of the different crops and land uses. Class definition has been done using photointerpretation techniques, using as a reference the building typologies defined in the SIOSE data model (Instituto Geográfico Nacional, 2007), differentiated by its use and its morphology: *isolated building, mixed urban, semi-detached house, detached house* and *industrial*. In order to

perform a more exhaustive description, urban building has been divided in *closed urban* and *historic*, according to the subdivisions of the mixed urban class in the SIOSE (some graphic examples are shown in Figure 16). Furthermore, necessary classes have been defined to perform a complete classification of the study areas: *arable lands* and *cultivated* and *tree crops*.

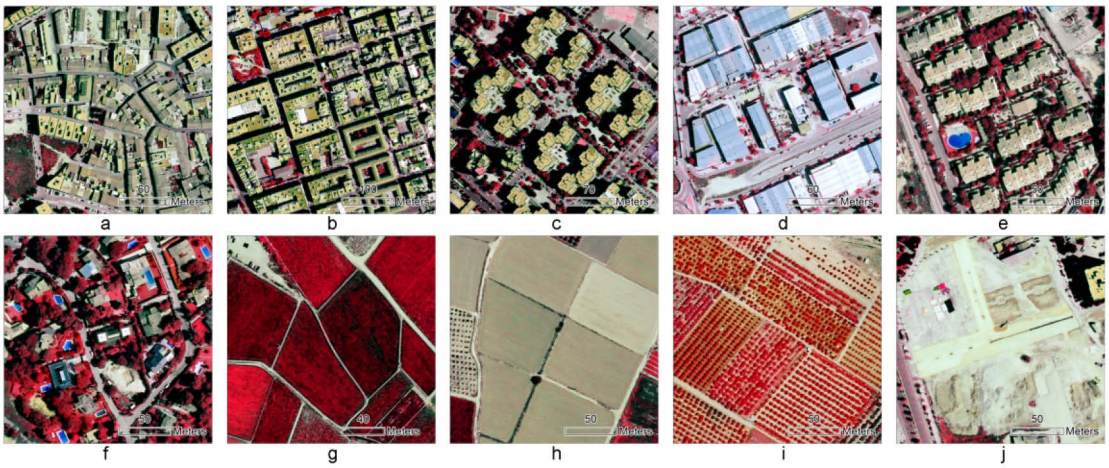

Figure 16. Examples of LU classes defined (Valencia area): historical (a), closed urban (b), open urban (c), industrial (d), semidetached housing (e), detached housing (f), cropland (g), arable land (h), citrus orchard (i), and bare soil (j).

In the case of the urban and rural classification study performed in Valencia, there are defined more detailed classes due to the variety of different building and agriculture classes existing in the area. The urban classes defined were: *historical buildings, urban buildings, open urban buildings, semi-detached houses, detached houses, industrial/warehouse buildings, religious buildings, commercial buildings, public buildings*, including schools, universities, sport facilities and civil and governmental buildings, and *gardens* and *parks*. The agricultural classes defined were: *arable lands, citrus orchards, irrigated crops, carob-trees orchards, rice crops, forest* and *greenhouses*.

4.2.2.2. Selection of descriptive features

In Table 2 and 0 the complete set of descriptive characteristics employed in the classification is shown:

Table 2. Descriptive features relative to the object.

Object features			
Group I	Spectral	Mean Infrared	*MeanIR*
		Std. Dev Infrared	*DesvIR*
		Min. Infared	*MinIR*
		Max. Infrared	*MaxIR*
		Mean Red	*MeanR*
		Std. Dev. Red	*DesvR*
		Min. Red	*MinR*
		Max. Red	*MaxR*
		Mean Green	*MeanG*
		Std. Dev. Green	*DesvG*
		Min. Green	*MinG*
		Max. Green	*MaxG*
		Mean NDVI	*MeanNDVI*
		Std. Dev. NDVI	*DesvNDVI*
		Min. NDVI	*MinNDVI*
		Max. NDVI	*MaxNDVI*
	Texture	Mean Border Intensity	*MeanIB*
		Std. Dev. Border Intensity	*DesvIB*
		Skewness	*Skewness*
		Kurtosis	*Curtosis*
		Uniformity	*Uniformidad*
		Entropy	*Entropia*
		Contrast	*Contraste*
		Inverse Moment of Difference	*IDM*
		Covariance	*Covar*
		Variance	*Varianza*
		Correlation	*Correlación*
Group II	Shape	Compactness	*CompacOB*
		Shape Index	*IFormaOB*
		Fractal Dimension	*DfOB*
		Area	*AreaOB*
		Perimeter	*PerimOB*
	Height	Mean Height	*MeanH*
		Std. Dev. Height	*DesvH*
		Max. Height	*MaxH*

Descriptive features relative to the internal and External context.

Internal context features			
Group III	Buildings	Mean Height	*MeanHED*
		Std. Dev. Height	*DesvHED*
		Max. Height	*MaxHED*
		Built-up Area	*SupED*
		Bulit-up Percentage Area	*BCRED*
	Vegetation	Mean Height	*MeanHV*
		Std. Dev. Height	*DesvHV*
		Mean NDVI	*MeanNDVIV*
		Std. Dev. NDVI	*DesvNDVIV*
		Percentage Area	*PercV*
External context features			
Group IV	Connectivity	Number of Relations	*Nrel*
		Mean Distance	*MeanDrel*
		Std. Dev. Distance	*DesvDrel*
	Urban morphology	Mean volumen per building	*VolM*
		Percentage of built area	*BCRSO*
		Built area	*SupEDSO*
		Mean building height	*MeanHSO*
		Std. Dev. Building height	*DesvHSO*
	Vegetation	Mean Height	*MeanHVSO*
		Std. Dev. Height	*DesvHVSO*
		Mean NDVI	*MeanNDVIVSO*
		Std. Dev. NDVI	*DesvNDVIVSO*
		Percentage Surface	*PercVSO*
	Shape	Compactness	*CompacSO*
		Shape Index	*IFormaSO*
		Fractal Dimension	*DfSO*
		Area	*AreaSO*
		Perimeter	*PerimSO*

Using the value of the 64 descriptive features obtained per object, their relevance in the classification procedure was studied using stepwise linear discriminant analysis. For this purpose, a training sample set of objects was used, computing the 64 descriptive features per object. In order to determine the most significant features, the sample set was analysed separately using the four defined feature groups, combined successively:

- Group I: level object features relative to the image information: spectral and texture.
- Group II: level object features relative to the geometry and height.
- Group III: internal object context features or sub-object features.
- Group IV: external object context features or block features.

Figure 17 shows graphically the global predicted accuracy when including features stepwise to the discriminant analysis classification for each defined feature groups. The use of the object descriptive features related to the image yields the highest global accuracy, reaching the 80% when up to 20 features are included in the discriminant model. The inclusion of new features do not seem to affect the predicted global accuracy of the model.

Geometric and height features produce the lower global accuracies, stabilizing their values around 50%. Meanwhile, the global accuracy of the features relative to the internal context becomes stable at 65%.

Features related to the external context make the accuracy stable around a global accuracy of the 70%. These features (build up area percentage, mean height and surface percentage covered by vegetation) have a synergic effect in the classification.

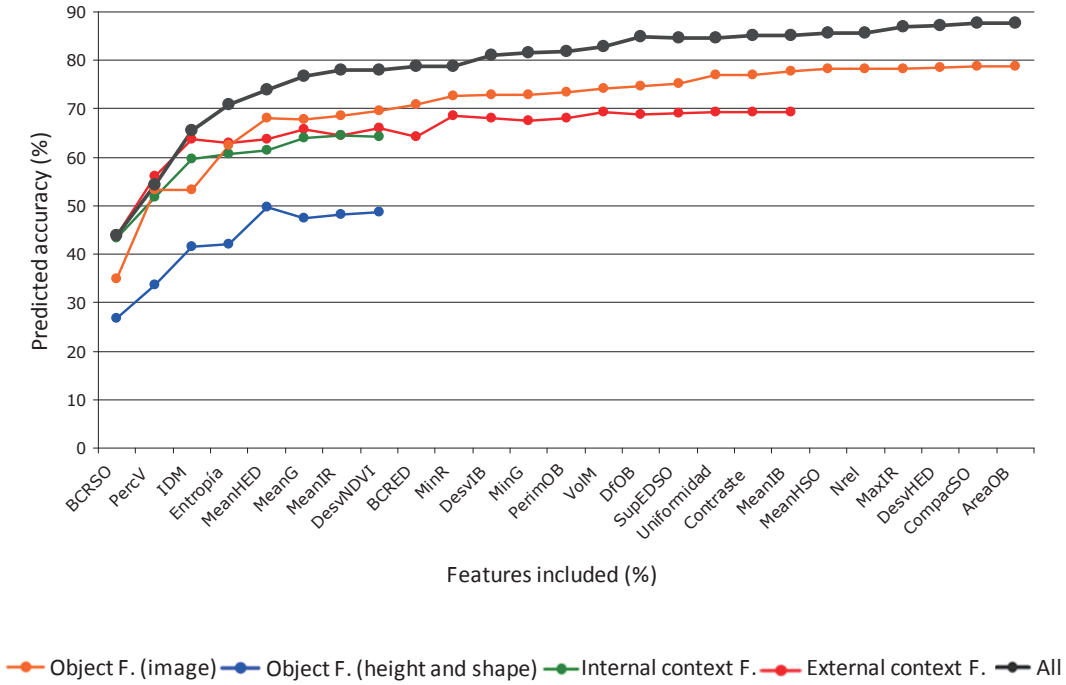

Figure 17. Predicted accuracy using stepwise linear discriminant analysis for the 25th first variables when combining all the groups compared to those obtained using independent variables. The names of the variables correspond to the features included when combining all the groups.

When combining all the descriptive features included in the discriminant analysis models of the defined groups, a synergic effect occurs, resulting in a significant increase of the global accuracy (see Figure 17). As features are progressively included in the model, there is an increase of the global accuracy. This accuracy represents an ascending trend that stabilises around the 85% of the variables added to the model.

4.2.2.3. Classification procedure

For classification, training samples were collected by assigning classes to objects (cadastral plots) by visual photointerpretation, applying two main criteria: representativeness of samples selected per class and homogeneity of the spatial distribution of samples in the study area. A restricted randomization scheme (Chatfield, 1991) was applied in this case, consisting of a random sample selection followed by a monitored sample reallocation and selection in order to maintain a minimum number of samples per class, to obtain a representative sample of each class, and to represent the changes in the area. As a result, 1,458 training samples were selected. A total of 128 objects (8.8%) of the samples corresponded to urban changes, concerning building construction, destruction, or use change.

Classification was carried out using decision trees constructed with the C5.0 algorithm (Quinlan, 1993), combined with the boosting technique. This algorithm divides the sample set by using mutually exclusive conditions, until homogeneous subgroups are generated, i.e. all the elements in a subgroup belong to the same class, or a stopping condition is satisfied. The stopping condition defined in this work is the minimum number of training cases that must follow each node. It was fixed to 5 cases, constraining the degree to which the initial tree fits the training data.

In order to maximize the efficiency of the number of available samples, the accuracy of the classification was assessed using leave-one-out cross-validation. This method uses a single observation from the original sample set as validation data, and the remaining observations as training data, iterating until each observation in the sample set is used for validation once. The evaluation of the classification was based on the analysis of the confusion matrix, which compares the class assigned to each sample to the reference class obtained by photointerpretation. From this confusion matrix, user's and producer's accuracies per class are computed, measuring the commission and omission errors, respectively.

4.3. Change detection

The method used in this study is based on combination of the two phases previously described (Figure 3), comparing classification of two different epochs or comparing the classification with a database. The evaluation of the change detection was evaluated as described in section 4.3.1.

4.3.1. Change detection evaluation

The sample selection was done using a semi-random sampling, ensuring minimum number of samples per class. Thus, the total number of samples was 1,458, from which 299 (20.5%) corresponded to changes between 2004 and 2008. Table 3 specifies the number of samples per class and time difference between epochs. The spatial distribution of the samples is shown in Figure 18.

Table 3. Evaluation samples from the area of Valencia.

		(to) 2008						
Reference		**arable**	**citrics**	**bare soil**	**historic**	**urban**	**suburban**	**industrial**
(from) 2004	**arable**	187	45	35		10		
	citrics	71	137	22		5		
	bare soil	1		82		44	35	10
	historic				213			
	urban			1		232		1
	suburban					1	221	
	industrial			15		3		87

Total number of samples = 1458

Total number of change samples = 299 (20,5%)

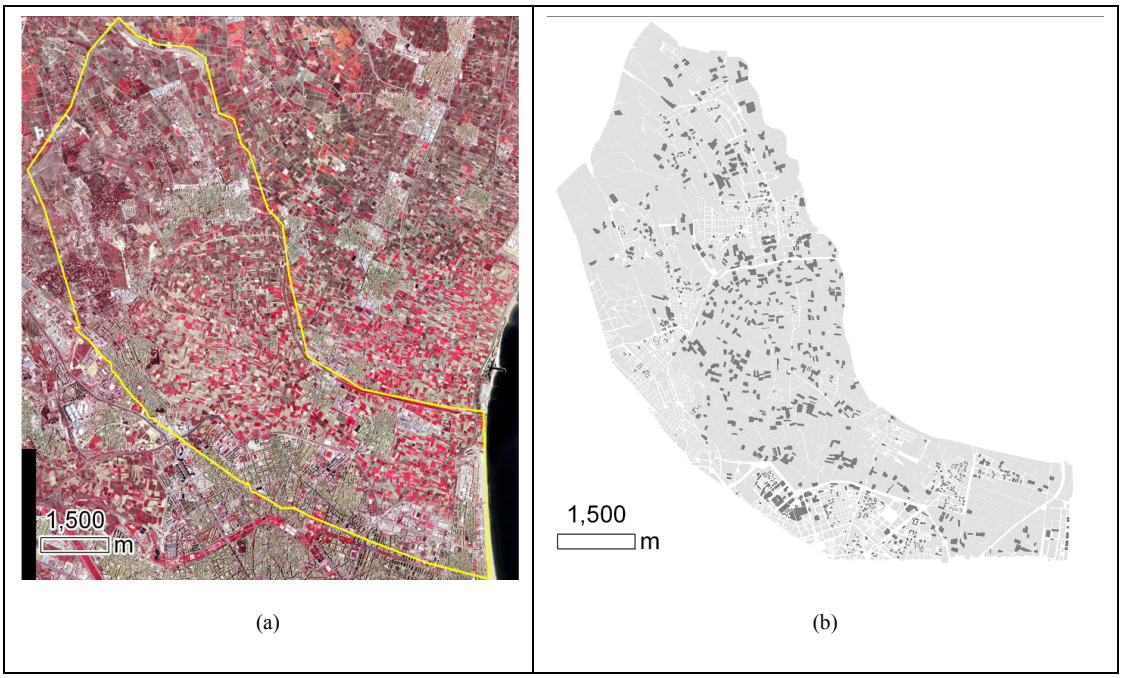

Figure 18. (a) Study area from the north area of Valencia (2008 PNOA orthoimage) and (b) distribution of selected samples within the study area.

The change detection efficiency is defined by adding the number of correctly detected changes to the number of correctly detected unchanged objects. Detectable errors are given when unchanged plots are wrongly detected as changed, whereas undetectable errors are produced when plots where changes occurred are detected as unchanged. The combination of detected changes and detectable errors composes the number of plots that would be manually reviewed in an updating process (Table 4).

Table 4. Distribution of chases and errors in the change detection assessment.

		Classification	
		Unchanged	Changed
Reference	Unchanged	**Coincidences**	**Detectable errors**
	Changed	**Undetectable errors**	**Detected changes**

5. Results

In this chapter, the results are divided attending to the two different phases: Phase I, to obtain the basic land cover classes; and Phase II, based on the multi-source attribute extraction and land use classification. Finally, results of the change detection procedure are shown.

5.1. Phase I results: generation of basic land cover classes

From the input data is obtained the segmentation using the Fuzzy K-Means, decomposing the image into homogeneous regions. The results of the segmentation can be seen in Figure 19.

(a)

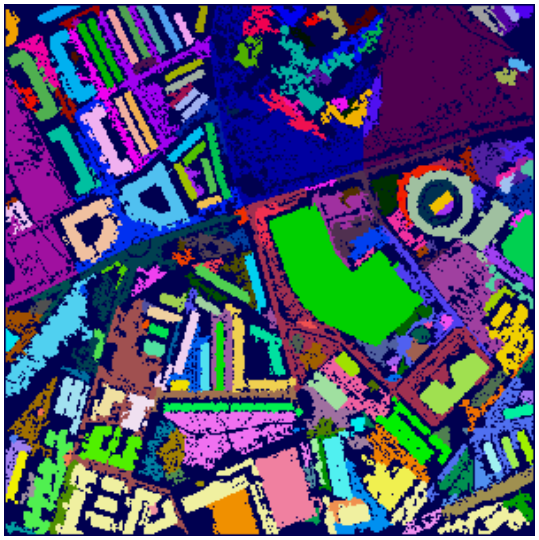

(b)

Figure 19. (a) study area from Alcalá (PNOA orthoimage) and (b) segmented image.

As can be noted, most of the shadows are detected as regions. Therefore, after the segmentation and the improvement of the classification, shadows must be eliminated. After the segmentation and the application of the simple rules with Dempster–Shafer theory to the FK-means segmentation, the result is an image classified in the basic land cover classes (Figure 20). The image can show false-positive water bodies in shadow regions, as discussed previously.

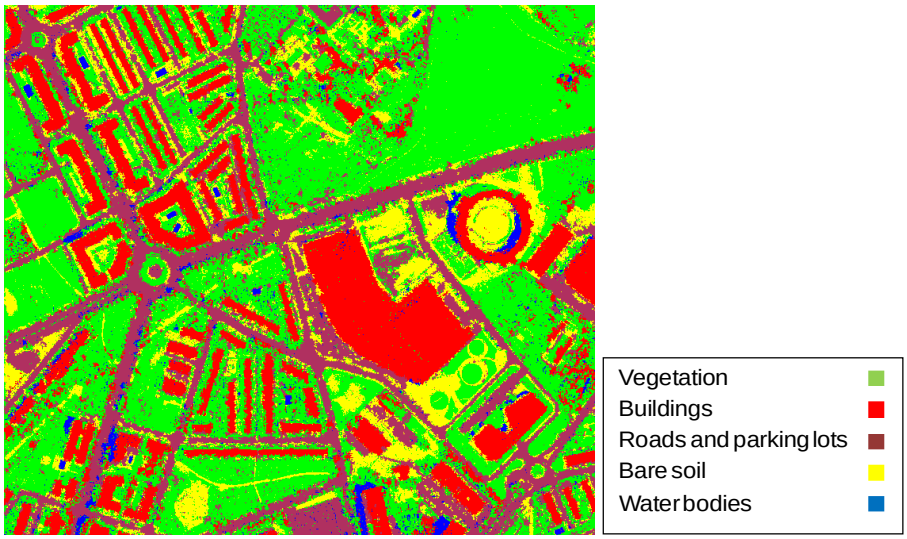

Figure 20. Initial LC classification with false-positives (some shadows have been assigned to water bodies).

These false-positives are corrected using the RAG; every shadow region is assigned to the class of the larger neighbouring region. This process will be improved in the near future, using Dempster–Shafer theory and optimized rules (Hermosilla et al., 2012b). If rule conflict occurs, Dempster–Shafer theory could help to solve the conflict using the orthogonal sum. However, simple rules established so far produce satisfactory results, as shown in some details of Figure 21.

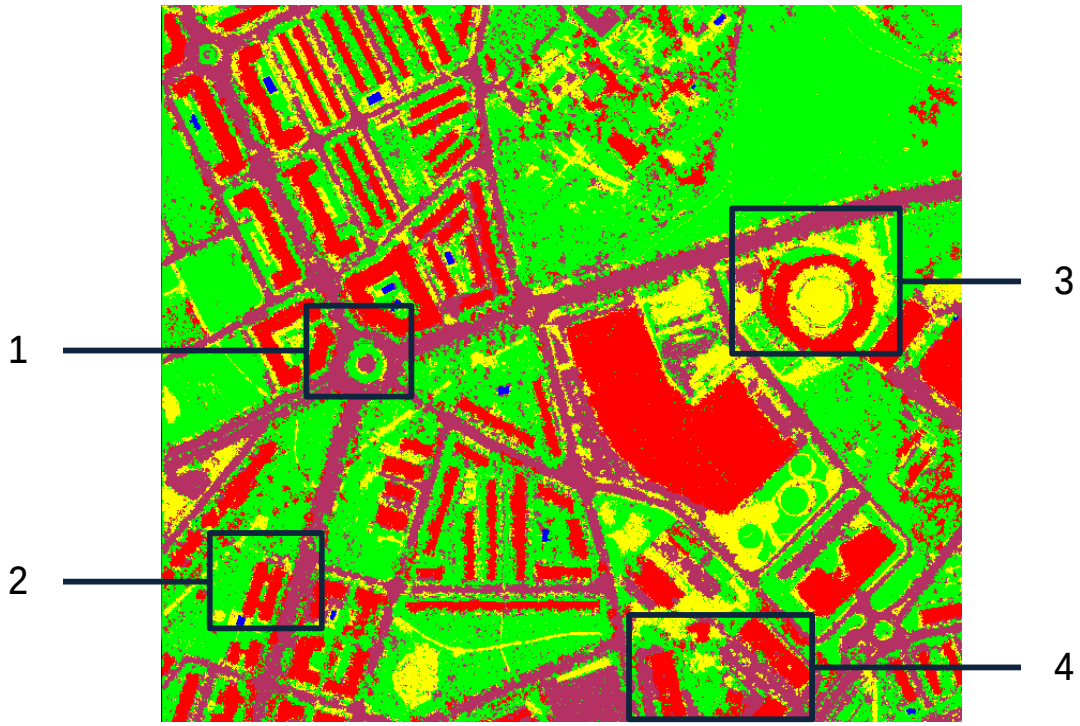

Figure 21. Classification with correction of the errors in the shadow regions.

Figure 22 shows four details, where false-positive water bodies due to shadow regions can be seen, and how they are corrected by means of assigning the class of the larger neighbour. Figure 22 (a,d,g,j) shows the details in the aerial PNOA image. In the second column, Figure 22 (b,e,h,k), the initial classification, with the false-positives for the water bodies; and finally, in the third column (Figure 22(c,f,i,l), how the method has corrected most of these false-positives.

The results shown in Figure 21 from the Alcalá area are difficult to evaluate numerically without reliable ground-truth data. A first visual analysis of the results shows that they are satisfactory, specifically in the classification of buildings and water bodies. With the objective of expressing a numerical result that quantifies the accuracy of the detection in comparison with a LULC database. The spatial classification produced by the proposed method (from PNOA and LiDAR images for 2010) was compared with the SIOSE polygons of the study area for 2005. The SIOSE assignment cannot be considered to be accurate or exact, because it is done by photo-interpretation and by round numbers; however, it will serve to contrast the differences between the two years (2005, 2010), and whether some changes have occurred.

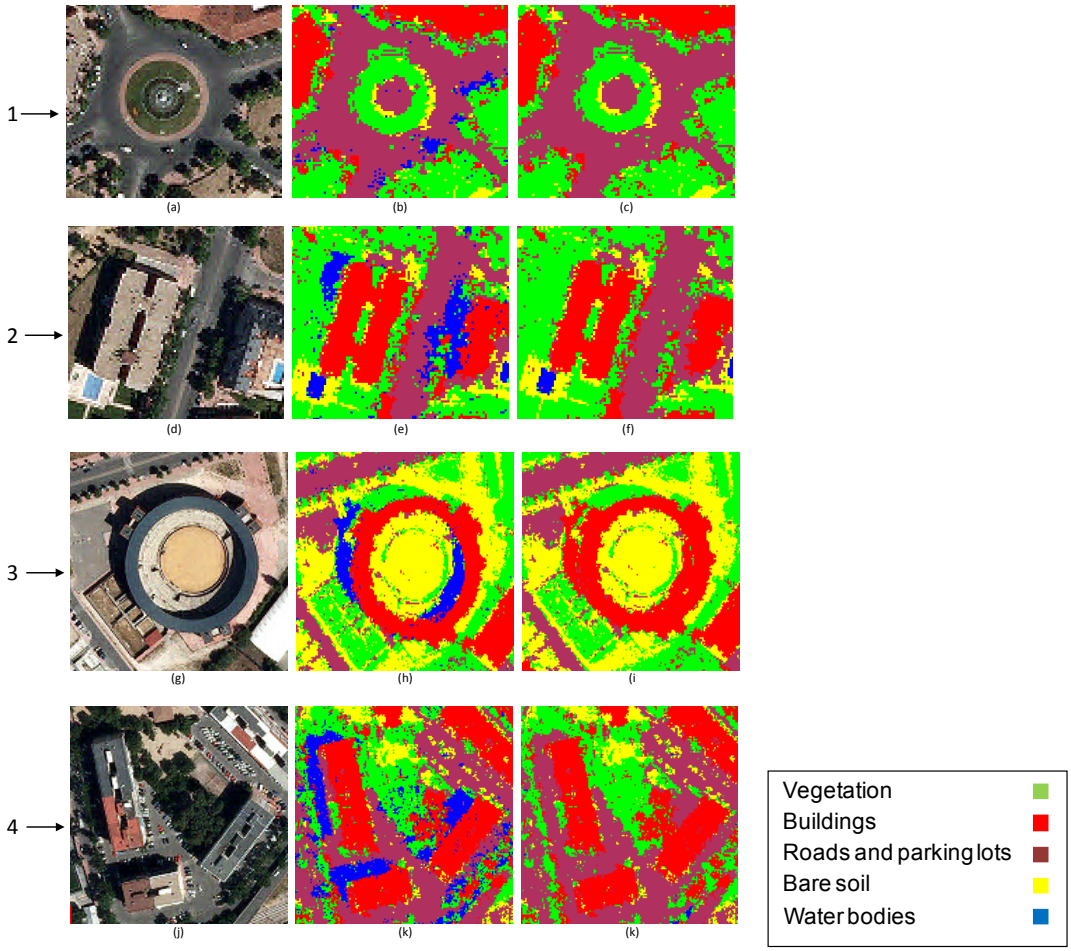

Figure 22. (a,d,g,j) Details of the aerial image PNOA; (b,e,h,k) corresponding basic land cover classification with false-positives for shadow regions; and (c,f,i,l) final results with shadow corrections.

The same procedure has been applied to the suburban area of Valencia for 2004 and 2008 Figure 23.a and Figure 24.a respectively). The results are shown in Figure 23.b and Figure 24.b. There have been many changes in this area between these two survey dates. Some buildings have disappeared (upper-right of the image) and others are new constructions (left part of the image). Note how the two roundabouts at the upper centre of the image, have been detected perfectly for both dates, even taking into account the different radiometry; therefore there is no change indicated in this respect. Other methods generally fail when the radiometry is so different.

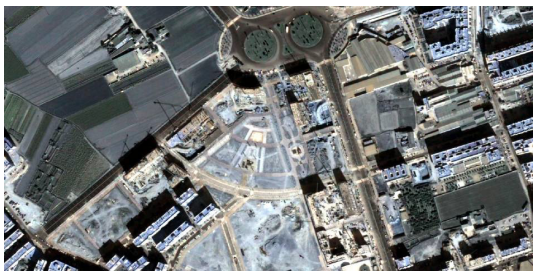

(a)

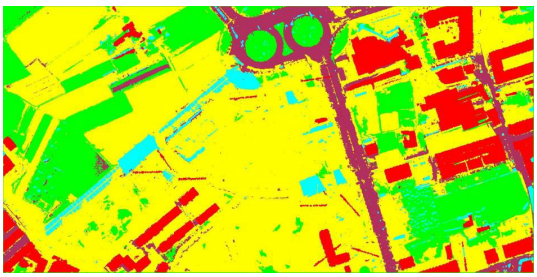

(b)

Figure 23. (a) Detail of the Qickbird image in 2004 and (b) classification of the image in 2004.

(a)

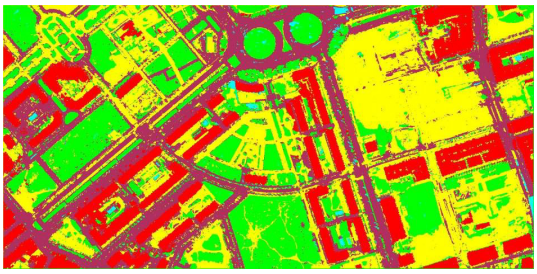

(b)

Figure 24. (a) Detail of the PNOA image in 2008 and (b) classification of the image in 2008.

5.2. Phase II results: multisource attribute extraction and land use classification

The phase II of the methodology was applied in the urban area of Valencia, obtaining an overall accuracy of 84.8%. In Figure 25, some examples of the classification in different areas are shown. For this area, the performed classification had a higher level of detail, introducing new sub-classes in both types of parcels (rural and urban).

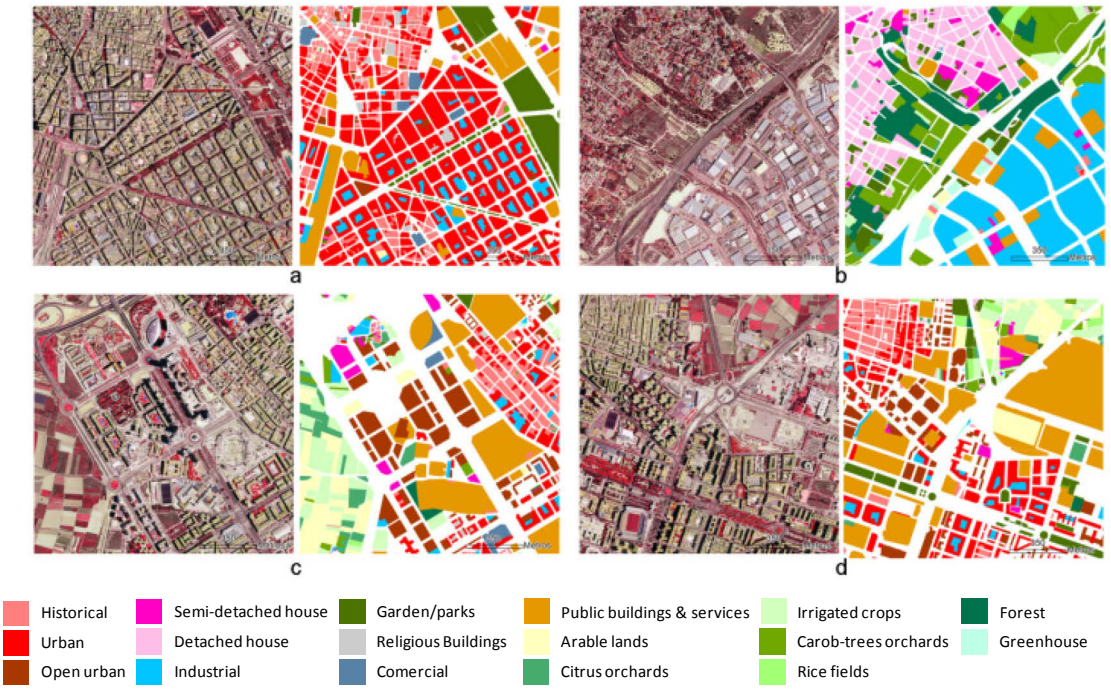

Figure 25. Examples of different areas of the urban area of Valencia with their classifications.

Per-class user's and producer's accuracies are high in the agricultural classes, reaching values higher than 90% in the case of *arable lands*, *citrus orchards*, *carob-trees orchards*, *rice crops*, *forest*, and slightly lower for *irrigated crops* (with values around 88% for both accuracies) and the user's accuracy of the class greenhouse.

Among the urban classes, the lowest accuracies and the most unbalanced values were obtained for classes *commercial* and *religious buildings*.

A graphical representation of the classification confusion matrix is shown in Figure 26.

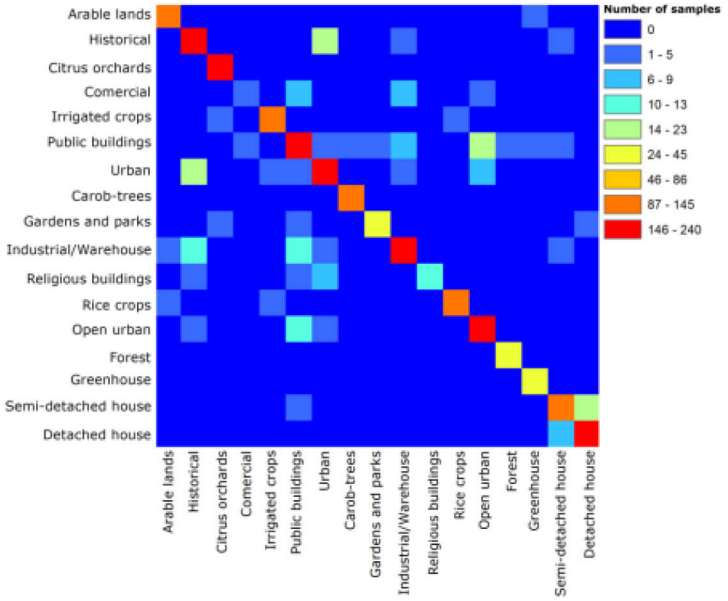

Figure 26. Graphic representation of the classification confusion matrix. Rows represent reference class and columns classified data.

The confusion matrix shows that *commercial buildings* had a poor performance and presented several misclassifications with *industrial/warehouse* and *public buildings* classes. *Religious buildings* class producer's accuracy reached a very low value (37%) due to the confusion with classes *urban* and *public buildings*. Medium user's and producer's accuracy values (70%) were achieved for *public buildings* and *semi-detached houses*. *Public buildings* presented a high degree of confusion with most of the building-related classes, due to their heterogeneity, and the fact that these buildings usually have significant morphological differences, producing misclassifications. Some particular *public building* plots containing covered sport facilities were erroneously assigned to *industrial/warehouse* buildings and vice versa. *Semidetached houses* were especially confused with *detached houses*, due to their obvious structural similarities. *Gardens* and *parks* presented unbalanced accuracies, due to the misclassification with *citrus orchards* and *public buildings*. Other building-related urban classes achieved better classification performances with slight confusions between them, being especially significant for the pair of classes *historical* and *urban*, as shown in the confusion matrix (Figure 26). In Figure 27 the user's and producer's classifications are shown.

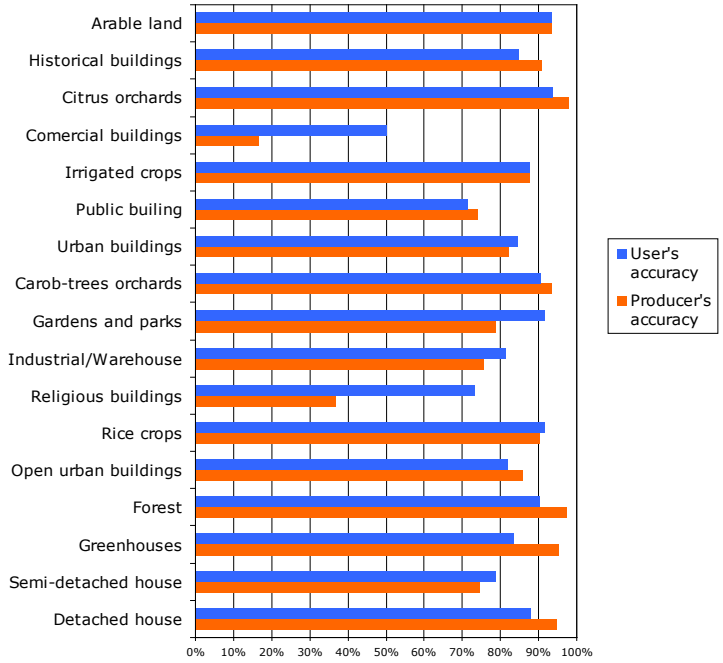

Figure 27. Classification user's and producer's accuracies for land use urban classes.

The urban classification of Valencia is shown in Figure 28.b. Figure 28.a corresponds to the PNOA image from 2008 in false infrared visualization.

(a)

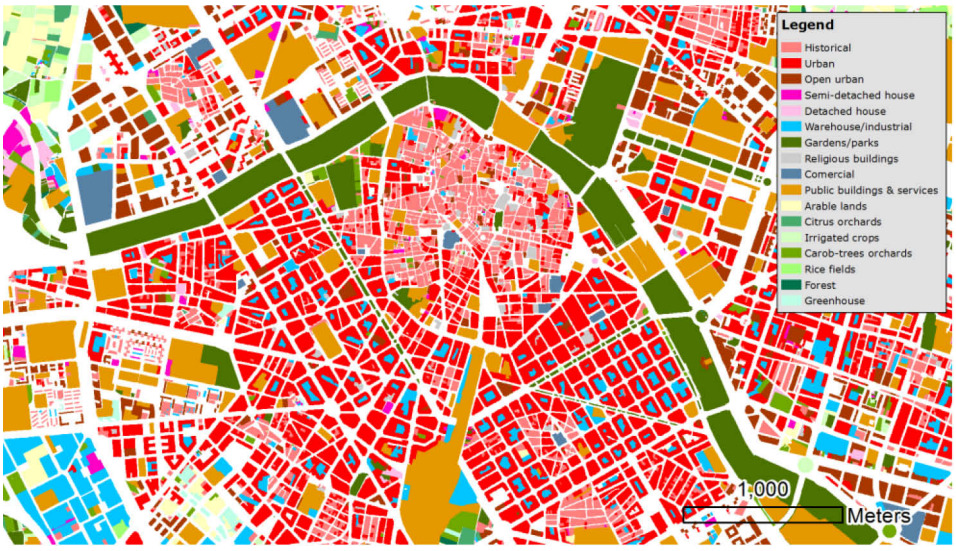

(b)

Figure 28. Land se classification of the city of Valencia.

5.3. Change detection results

5.3.1. Change detection in periurban areas

Change detection results are shown in Table 5. The global rate of correctly detected changes or no-changes is 98.7%. The percentage of objects (cadastral parcels, polygons, etc.) to be visually reviewed by photointerpretation and field visits in a hypothetical change detection procedure at production level would be 9%, mostly corresponding to plots with actual changes (8.1%). Height information provided by the nDSM is critical to discriminate between different building typologies, and between buildings from bare soil, correcting most of the detectable and undetectable errors and improving the performance of the change detection process. Figure 29 shows an image detail of the study area and the change detection represented for the selected samples in a comparative test carried out with and without considering 3D data, where the significant reduction of undetectable errors and the increase of detected changes are perceptible. These results are shown in Figure 30, where LiDAR derived information allows to reduce both, commission (orange) and omission (red) errors, increasing the rate of detected changes.

Table 5. Change detection assessment concerning urban-related changes.

		With LiDAR data	
		Unchanged	Changed
Reference	Unchanged	**90.6%**	**0.9%**
	Changed	**0.4%**	**8.1%**

Figure 29. Detail of the study area in infrared colour composition for the years 2004 (a) and 2008 (b); and maps showing change detection results of samples without considering (c) and considering (d) 3D features.

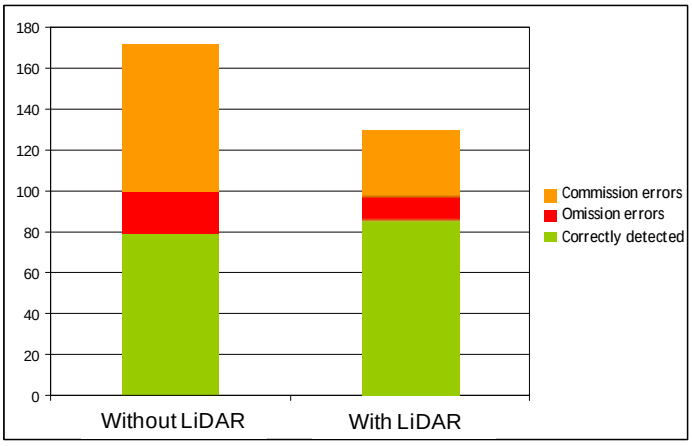

Figure 30. Change detection method comparison using or not using LiDAR.

5.3.2. Change detection in rural areas

Change detection method was also performed in rural areas from Murcia (Figure 31), where targeted changes where searched. These changes were *new irrigation pools, crops removal* and *new crops*. Due to the low number of the new irrigation pools, this class was not evaluated.

Figure 31. Detail of the PNOA image from 2008 of the testing area of Murcia.

The results of the evaluation are shown in Table 6. From 159 testing plots of the *crops removal* type, 140 changes were detected, which means an omission error of 19 (changes not detected). For the *new crops* type, from 220 changes, 196 were correctly detected, leaving 24 parcels where no change was detected. Therefore, the total accuracy rate of change detection in the rural area was 89.09%, considering new crops and crops removal. In Figure 32, the number of detected and not detected changes for the two change typologies can be seen.

Table 6. Results of the evaluation of the change detection method in rural areas.

	Changes	Detected	Not detected	% success
Crops removal	159	140	19	88.05%
New crops	61	56	5	91.80%
Total	**220**	**196**	**24**	**89.09%**

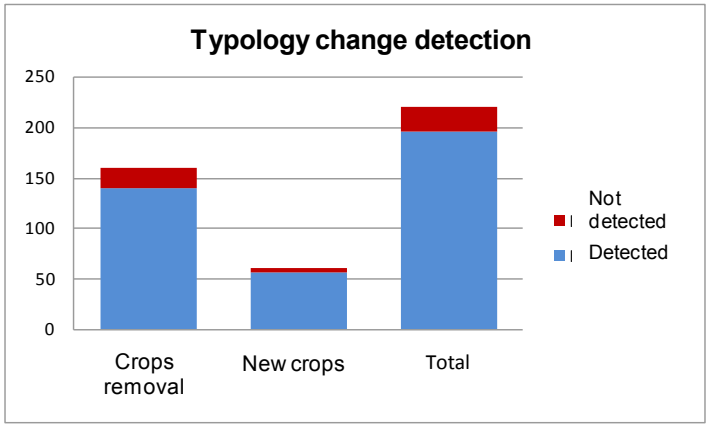

Figure 32. Changes detected and not detected of the two evaluated change types.

The total number of changes detected in the rural area is shown in Table 7 from a total of 39,964 studied parcels. In Figure 33, two details of the changes detected in the rural area are shown.

Table 7. Change detection values.

	Nº of changes detected
New irrigation pools	17
Crops removal	2172
New crops	1631
Total changes	**3820**

Figure 33. Two details of changes detected.

5.4. Application to quantify polygon attributes in SIOSE database

The spatial classification produced by the first part of proposed methods (generation of basic land cover classes) was compared to the SIOSE polygons of the urban study area of Alcalá for 2005. The SIOSE assignment cannot be considered to be accurate or exact, because it is done by photo-interpretation and by round numbers (multiples of 5); however, it will serve to contrast the differences between the two epochs (2005, 2010), and whether some changes have occurred.

Table 8. Change detection values for polygon 104.

	% Proposed method	% SIOSE
Buildings	38.6	80
Vegetation	27.5	10
Roads	23.7	5
Bare soil	9.3	0
Water bodies	0.9	5

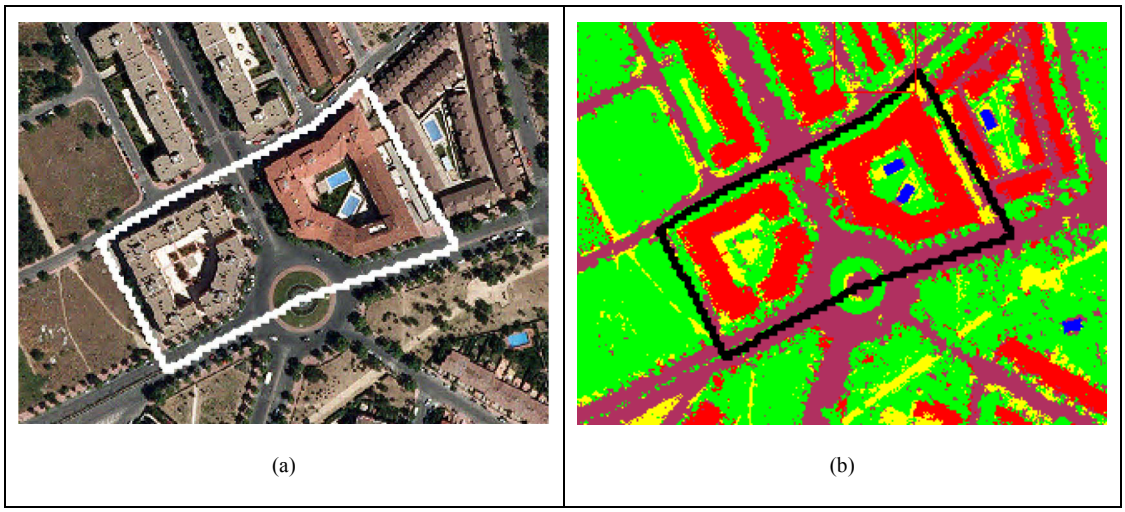

(a) (b)

Figure 34. SIOSE polygon 104 (a) over the PNOA image and (b) over the LC classified image.

At first sight, the results obtained by the proposed method for polygon 104 (Figure 34) differ from those obtained manually by the operator when the SIOSE data was classified in 2005 (Table 8). While the SIOSE assigned 80% building coverage to this polygon, 10% for vegetation, 5% for roads, and 5% for swimming pools, the proposed method assigned around 40% for buildings, 25% for vegetation, 25% for roads, 10% for bare ground, and 1% for water bodies or swimming pools. If we assume that there was no change within this polygon between 2005 and 2010, we can analyze the differences visually. The 80% percentage for buildings assigned by SIOSE appears excessive, and the 40% calculated by the proposed method would be more accurate. Similarly, the vegetation- and road coverage calculated by the proposed method seems to be more realistic than the values provided by SIOSE. However, in the case of vegetation, it is more difficult to decide which value is more reliable; visually, it appears to be higher than the 10% assigned by SIOSE; however, the 25% indicated by the proposed method could be too high, because the shadow regions are considered as vegetation whereas they could be other coverage types (roads or bare ground). Finally, for the water bodies, there is a 4% difference between the proposed method and the SIOSE. This is due to the SIOSE rounding up the coverage percentages to multiples of 5, whereas the proposed method determines a more precise percentage. Therefore, for polygon 104, the human operator for SIOSE estimated 5% water coverage, which is the minimum percentage for SIOSE, whereas the proposed method has estimated 1% coverage.

Table 9. Change detection values for polygon 127.

	% Proposed method	% SIOSE
Buildings	27.9	75
Vegetation	45	10
Roads	19.4	10
Bare soil	7.2	0
Water bodies	0.5	5

(a)

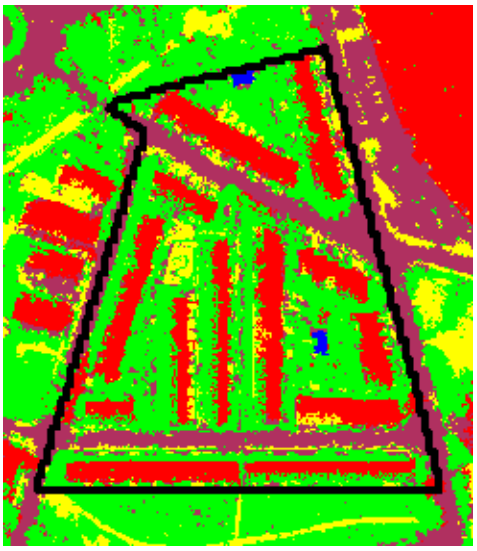

(b)

Figure 35. SIOSE polygon 127 (a) over the PNOA image and (b) over the LC classified image.

As with polygon 104, there appear to be important differences in polygon 127 (Table 9 and Figure 34) between the percentages assigned by the manual SIOSE process and the automatic process of the proposed method. Although, visually, it could seem that the building coverage assigned by SIOSE is too high (75%, versus 30% using the proposed method), the SIOSE estimate could be more accurate in this case. The proposed method shows vegetation coverage for some regions that actually correspond to small detached or semidetached houses of low elevation. Similarly, the 45% vegetation coverage estimated by the proposed method seems to be higher than reality. However, the percentage of 10% given by SIOSE seems to be a slight underestimate, compared to what can be seen in the aerial image from 2010, although it could be accurate for 2005.

The 10% difference in road coverage could be explained by the greater precision of the proposed method, compared with the manual SIOSE classification; or because this difference represents a real change between 2005 and 2010. SIOSE does not indicate bare soil coverage in this polygon, while the proposed method indicates 5% coverage; this could be the difference between the two survey years. The difference for water coverage could be explained in the same way as for polygon 104.

In the same way, comparison with SIOSE polygons was done using the multi-source attribute extraction and land use classification in the urban area of Valencia.

Although the SIOSE database indicates a unique edification typology, it is produced an exception in the case of the class *mosaic*. The *mosaic* is defined as *coverage* union (land uses) which geometrical distribution and division between them is clearly perceptible. In practice, in urban areas *mosaics* contain polygon groups whose areas are less than the minimum, and these are generally isolated from the population centres surrounded by farmlands.

Figure 36 shows an example of a SIOSE polygon and the result after object classification. This example is a *mosaic* type polygon where industrial and urban land-uses are distinguished and where the area covered by buildings are detailed: *planned urban* and *industrial*. When combining building detection techniques and object-based automatic classification, four different types of buildings can be distinguished. Thus, a more accurate estimation of the build up area is achieved than that registered in the SIOSE.

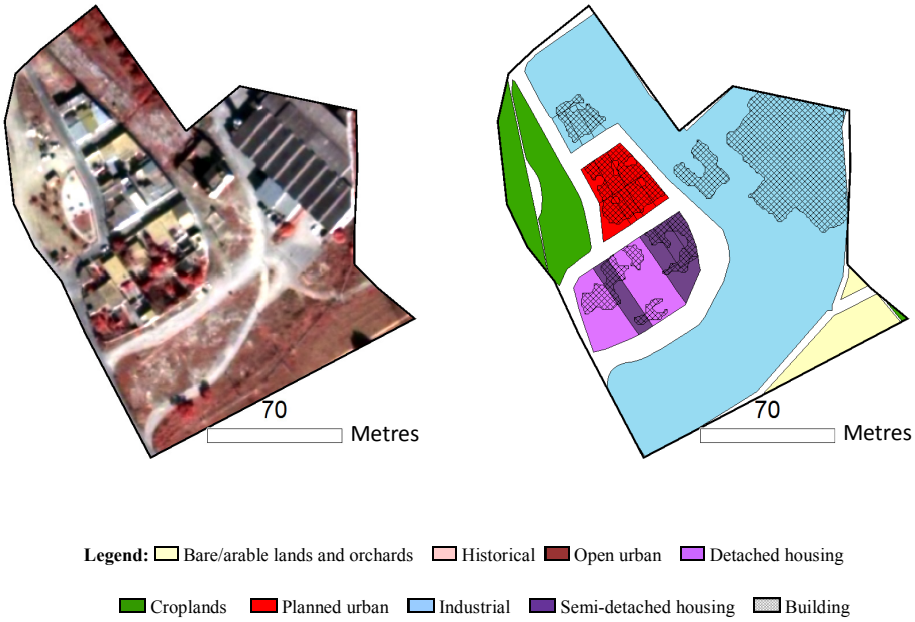

SIOSE		Classification	
Build up area	***50.5%***	***Build up area***	***21%***
└ 55%	Planned urban	└ 69,1%	Industrial
└ 45%	Industrial	└ 15,7%	Planned urban
		└ 8,4%	Semi-detached housing
		└ 6,9%	Detached housing

Figure 36. Image, classification results and build up area percentage described in the SIOSE and automatically estimated (total and per class) from a mosaic type polygon where urban from industrial uses can be distinguished.

Although there are two building classes in the mosaic, usually the drawn SIOSE polygons in urban areas only inform about a unique class, with the consequent loss of detail. For example, in Figure 37 a characteristic SIOSE polygon in a planned urban area is represented. These areas are basically composed of *planned urban* buildings, but often coexist with other building typologies such as *isolated buildings*, *detached houses* or even *industrial* buildings. The use of automatic classification techniques allows a more detailed typology disaggregation, which means a more complete description of the polygon.

The coexistence between *planned urban* and *historic*, and the fact that the contiguous polygon belong to a *historic* use, points out that the SIOSE polygon geometry analysed could be redefined according to the classification results, so that the buildings of each polygon could present a major homogeneity in their typologies. Thus, the use of automatic techniques would simplify the automatic SIOSE polygon delimitation with a better objectivity than visual perception techniques over areas with difficult discrimination, as in the case presented in Figure 38.a and Figure 38.b, both belonging to the boundaries of the SIOSE polygon showed in Figure 37.

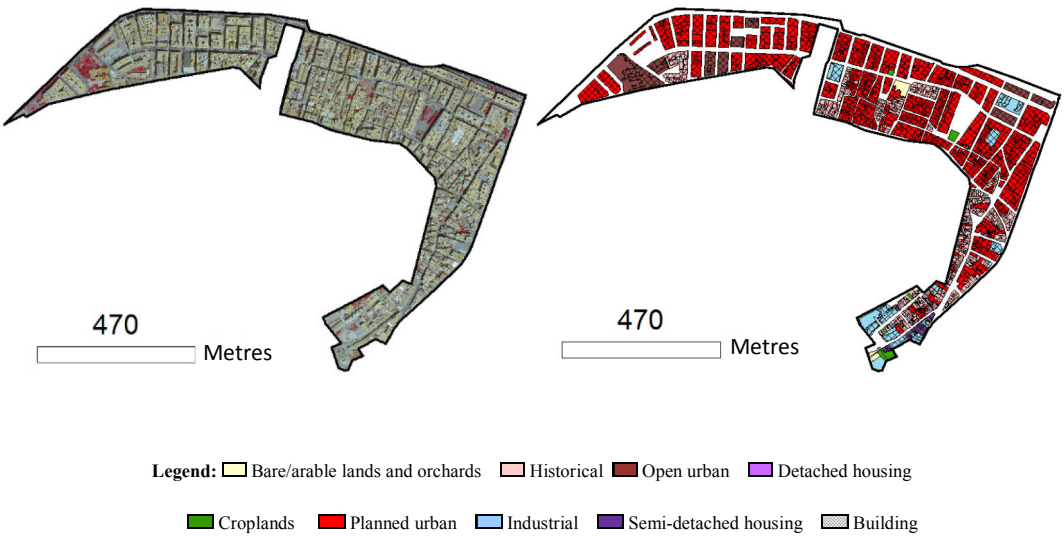

SIOSE	**Classification**
Build up area 75%	***Build up area 69%***
100% Planned urban	71,1% Planned urban
	15,5% Historical
	7,4% Open urban
	5,1% Industrial
	0,9% Semi-detached housing

Figure 37. Image, classification results and build up surface percentage described in the SIOSE and automatically estimated (total and per class) from an urban planned polygon.

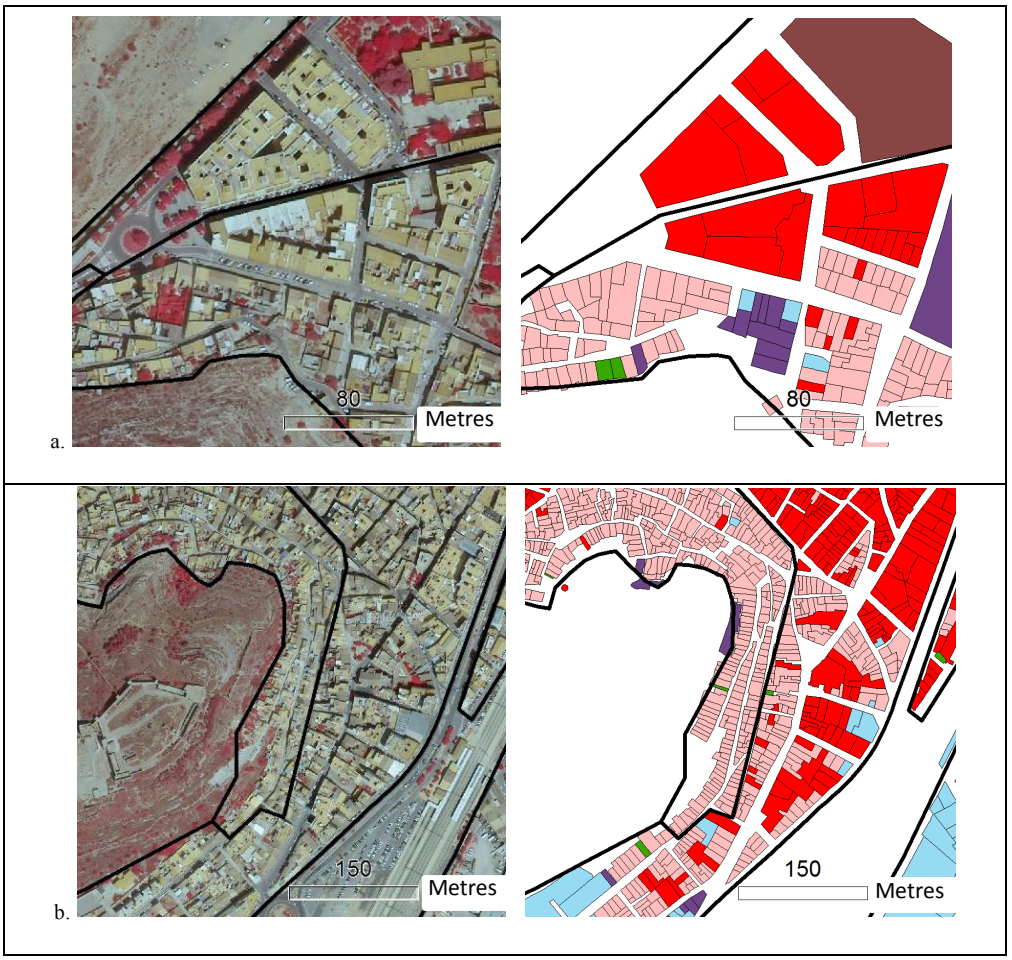

Figure 38. Example of areas where the automatic classification could help in the definition of the SIOSE polygons (which boundaries are represented with black colour lines).

Presented examples show the potential of the automatic methodologies of building detection and land-use classification employing remote sensing data for the estimation and calculation of useful parameters for the geo-spatial land-use/land-cover database creation/update. Results show a higher accuracy and higher detail level than the obtained when using photointerpretation methods, which enable a more objective and deeper characterisation of the urban classes in urban and periurban areas.

6. Conclusions

A semi-automatic method has been proposed for object-based classification of images and change detection at two levels of thematic detail.

During the first phase of the methodology, the RAG data structure allows the introduction of topological properties that are used to improve the initial segmentation of the image. Dempster–Shafer theory allows an improvement of the initial segmentation and classification.

In the second phase, the exhaustive set of features extracted per object including spectral, texture, shape, 3D, internal and external context indices, enables a complete description of objects to obtain high accuracy classification results.

The proposed methodology can determine the percentage coverage for SIOSE polygons, being useful for change detection and database updating.

Future works should be focused in the integration of Dempster–Shafer theory and decision trees, as well as the application of direct classification techniques for change detection, extended to a broader variety of areas and landscapes.

7. Future Studies

During last years, pixel-based change detection methods have been used for change detection in objects. Berberoglu and Akin (2009) describe various change detection methods such as Change Vector Analysis (CVA), image rationing and image differencing, using an object-oriented classification in order to increase precision and to reduce the time of classification.

The most widespread object-based classification methods usually start from a multitemporal segmentation of multispectral images. In this procedure images from different epochs are segmented in order to obtain the difference between them and/or the information that contain in the time interval of the images. Gamanya et al. (2009), for example, segments the images using multispectral features, textures, object size and behaviour at different scales in different epochs to compare and classify them. Thus, changes can be detected between the segments of the two studied epochs. In a similar way, Huang et al. (2010) performs image segmentation from two epochs using textures and intensities. Then, changes occurred between the segments are obtained using a segmented image differentiation.

As noted, segmentation is common in several works, but some modifications are noticed in the change detection procedures, such as in Niemeyer et al. (2007), that use correlation variables for the segment comparison, or in Bontemps et al. (2008), where a classification is done on the basis of a previous object definition rules before the differentiation.

Other procedures are focused in the element classification from different epochs. In Hall and Hay (2003), despite performing a segmentation using various scales, each segment is classified using the mean of its pixel values, and later with the classified segments, the difference between

the two epochs is calculated. There are cases where the segmentation is not necessary because the object, or the study elements, are already classified and belong to a GIS or to a database. To update these elements using remotely sensed images, a classification is obtained with the classes contained in the database and then, the classification is compared with the original class of the objects (Walter, 2004).

Until now the work performed has been based in the information contained within the objects. Sometimes external variables from the objects have been studied for the multitemporal image differencing, like in Im et al. (2008). In this work, the neighbour correlation has been studied for each object on the image. In this case, change detection is based in the correlation of the multispectral values in the same area, that in comparison with another image of a different epoch, the correlation will be higher when there are no changes and lower when changes have occurred.

Methodologies currently posed for change detection use multispectral data or LiDAR data independently. Change detection methodologies which combine both data types are being developed, as well as methodologies that take into account shape, context and internal object information. Even though processes that combine both information types can be found, none of them are object-based.

In the framework of our EuroSDR project, some experiments were done using pixel-based change detection methods applied to objects. The methods used were principal components analysis (PC) and change vector analysis (CVA).

PC analysis allows detecting when analysing secondary components, the objects that have change respect to those unchanged. Using PC, have been tested specific relationships between changes in rural areas. The test was done over parcels with great homogeneity within them, which made their differentiation easy.

In Figure 39, the changed (red) from unchanged objects (blue) can be distinguished in the scatterplots, as well as its typology: from vegetation to bare soil and vice versa, where highest red coloured groups represent the change from vegetation to bare soil and the lowest red group are the new vegetated parcels for the PC 2, 3 and 5. This suggests the possibility of discrimination between these two classes.

The CVA consists in the calculation of the module and direction of the vector that joins pixel values in a space defined by two or more variables in two different epochs. The module value is referred to the change magnitude, and the direction represents the type of change. Scatterplots between the change direction and magnitude were analysed in a normalised scale from 0 to 1.

In Figure 40, the scatterplot that represents the direction versus the distance from changed (red) and unchanged (blue) objects is shown. Objects tested belong to the same rural area used for the PC analysis, where the parcels used were homogeneous. The homogeneity of the parcels allows clearly to detect and to define the changes in two specific areas from the scatterplot. Direction values around 150º, are those parcels with change from vegetation to bare soil and vice versa for the parcels located around 350º. Both changes present distance values higher than 0.25.

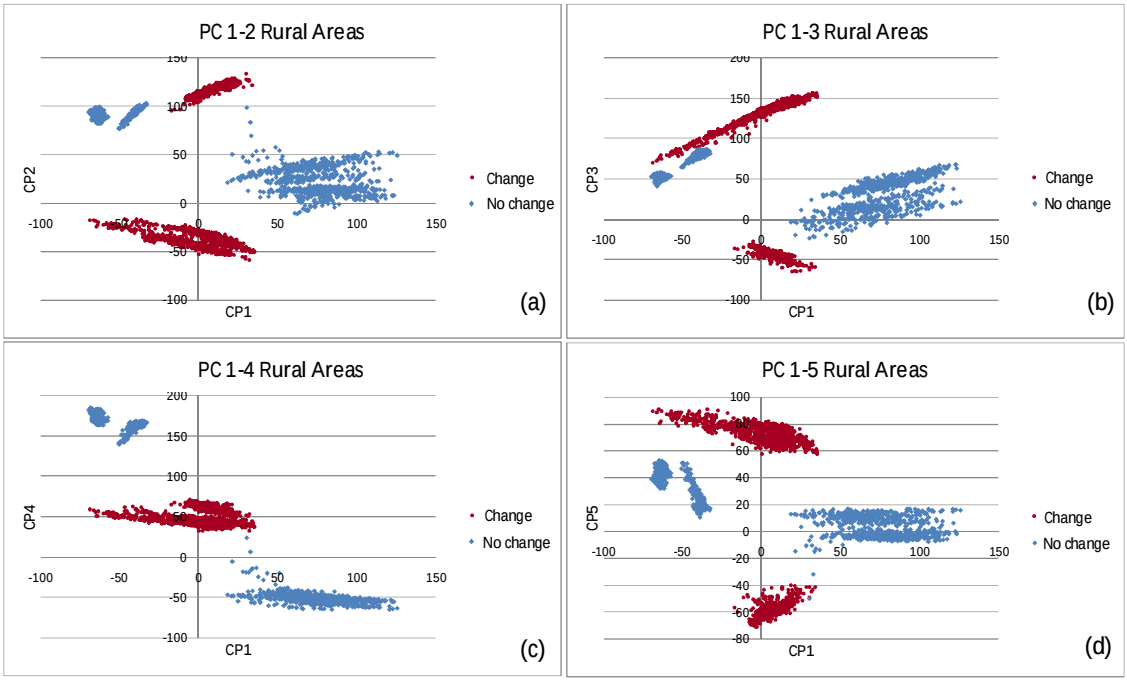

Figure 39. Scatterplot comparing PC 1 and 2 (a), 1 and 3 (b), 1 and 4 (c) and, 1 and 5 (d) for a rural area.

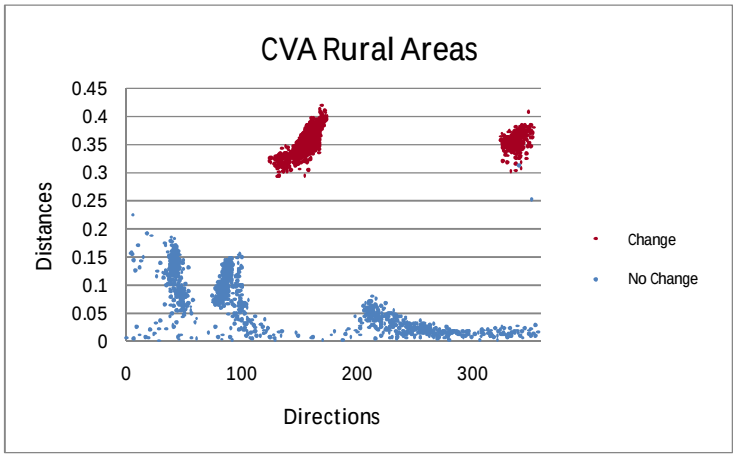

Figure 40. Scatterplot of the change vector in a rural area.

These standard change detection methods applied over objects do not have precise results, but present several possibilities in order to complement the methodology developed, adding new information per feature or helping to the direct change detection.

8. References

Arozarena, A., Villa, G., 2005. Plan Nacional de Ortofotografia Aerea de Espana (PNOA). (Spanish national plan of aerial orthophotos) Topografía y cartografía: Revista del Ilustre Colegio Oficial de Ingenieros Técnicos en Topografía, 22, pp. 30–41.

Balaguer, A., Ruiz, L.A., Hermosilla, T., Recio, J.A., 2010. Definition of a comprehensive set of texture semivariogram features and their evaluation for object-oriented image classification. Computers and Geosciences, 36, 231-240.

Berberoglu, S., Akin, A., 2009. Assessing different remote sensing techniques to detect land use/cover changes in the eastern Mediterranean. *International Journal of Applied Earth Observation and Geoinformation.* 11 (1), 46- 53.

Bins L.S., García Fonseca, L.M., Erthal, G.J., Mituso, F. 1996. Satellite imagery segmentation: a region growing approach, VIII Simposio Brasileiro de Sensoramiento Remoto, pp. 677 – 680.

Bogaert, J., Rousseau, R., Hecke, P.V., Impens, I., 2000. Alternative Area-perimeter Ratios for Measurement of 2D Shape Compactness of Habitats. - Applied Mathematics and Computation 111 (1): 71-85.

Bontemps, S., Bogaert, P., Titeux, N., Defourny, P., 2008. An object-based change detection method accounting for temporal dependences in time series with medium to coarse spatial resolution. *Remote Sensing of Environment.* 112 (6), 3181- 3191.

Canty M. J., Nielsen, A.A., 2006. Visualization and unsupervised classification of changes in multispectral satellite imagery. International Journal of Remote Sensing 27(18), pp. 3961-3975.

Chatfield, C., 1991. Avoiding Statistical Pitfalls. - Statistical Science 6 (3): 240-252.

Dempster, A.P., 1968. A Generalization of Bayesian Inference, Journal of Royal Society, 30, pp. 205 – 247.

Duda, T., Canty, M., 2002, Unsupervised classification of satellite imagery: Choosing a good algorithm, 23(11), 2193 – 2212.

Estornell, J., Ruiz, L.A., Velázquez-Martí, B., Hermosilla, T., 2011. Analysis of the factors affecting LiDAR DTM accuracy in a steep shrub area. International Journal of Digital Earth, 4 (6), 521-538.

Gamanya, R., Maeyer, P. D., Dapper, M. D., 2009. Object-oriented change detection for the city of Harare, Zimbabwe. *Expert Systems with Applications.* 36 (1), 571- 588.

Hall, O., Hay, G. J., 2003. A Multiscale Object-Specific Approach to Digital Change Detection. *International Journal of Applied Earth Observation and Geoinformation.* 4 (4), 311- 327.

Haralick R.M., Shapiro, L.G., 1985. Image Segmentation techniques, Computer vision graphics and image processing, 29, pp. 100 – 132.

Haralick, R.M., Shanmugan, K., Dinstein, I., 1973. Texture Features for Image Classification. - IEEE Transactions on Systems, Man and Cybernetics 3: 610-621.

Hermosilla, T., Gil-Yepes, J.L., Recio, J.A., Ruiz, L.A., 2012a. Change detection in periurban areas based on contextual classification. Photogrammetrie, Fernerkundung & Geoinformation (PFG), 2012 (4), 359-370.

Hermosilla,T., L.A. Ruiz, J.A. Recio, M. Cambra-López, 2012b. Assessing contextual descriptive features for plot-based classification of urban areas. Landscape and Urban Planning 106, pp. 124– 137. (CAmbiar en el texto la a por la b y viceversa)

Huang, L., Zhang, G., Yang, L.I., 2010. An object-based change detection approach by integrating Intensity and texture differences. *Informatics in Control, Automation and Robotics (CAR), 2010 2nd International Asia Conference*, 258-261.

Im, J., Jensen, J., Tullis, J., 2008. Object-based detection using correlation image analysis and image segmentation. *International Journal of Remote Sensing*, 29 (2), 399-423.

Instituto Geográfico Nacional, 2007. Sistema de información de ocupación del suelo en España. *Manual de Fotointerpretación. Versión 1.2.*

Jain R., Kasturi, R., Schunck, B.G., 1995. Machin Vision, New York, McGraw Hill Science.

Klir, G.J., Wierman, M.J., 1999. Uncertainty-Based Information: Elements of Generalized Information Theory. Springer.

Kohlas J., Monney, P.A., 1995. A mathematical theory of hints: An approach to the Dempster–Shafer theory of evidence. Berlin: Springer-Verlag.

Krummel, J.R., Gardner, R.H., Sugihara, G., O'Neill, V., Coleman, P.R., 1987. Landscape Patterns in a Disturbed Environment. - OIKOS 48 (3): 321–324.

Laurini, R., Thompson, D., 1992. Fundamentals of spatial information (Vol. 5). *London, UK, Academic Press.*

Leblon B., L. Gallant and H. Granberg, "Effects of shadowing types on ground-measured visible and near infrared shadow reflectances", Remote Sensing of Environment, 58(3), 1996, pp. 322 - 328.

Malpica J.A., Alonso, M.C., Sanz, M.A., 2007. Dempster-Shafer theory applied to image fusion in a Geographic Information Systems: A survey. Expert Systems with Applications 32 (1) pp: 47-55.

Malpica, J.A., Alonso, M.C., Papi, F., Arozarena, A., Martínez de Agirre, A., 2012. Change detection of buildings from satellite imagery and LIDAR data, International Journal of Remote Sensing 2012 (in press).

Martínez de Agirre A., Malpica, J.A., 2012. Detecting shadows in a segmented land used land cover image with LIDAR data, Proc. of the IEEE International Geoscience and Remote Sensing (IEEE Xplore), pp. 5468-5471.

Martinez de Agirre, A., Malpica, J.A., 2010. Constructing a Digital Terrain Model from LIDAR data. In the book Advances in Geoinformation Technologies, edited by Jiri Horak, Lena Halounova, Tomas Hlasny, Dagmar Kusendova and Vit Vozenilek. Institute of Geoinformatics. Czech Republic.

McGarigal, K., Marks, B.J., 1995. FRAGSTATS: Spatial Pattern Analysis Program for Quantifying Landscape Structure. - General Technical Report PNW-GTR-351, U.S. Department of Agriculture, Forest Service, Pacific Northwest Research Station, Portland, OR, USA: 122pp.

Mena, J.B., Malpica, J.A., 2005. An automatic method for road extraction in rural and semi-urban areas starting from high resolution satellite imagery. Pattern Recognition Letters, 26, pp: 1201-1220.

Niemeyer, I., Marpu, P.R., Nussbaum, S., 2007. Change detection using object features. *Geoscience and Remote Sensing Symposium, 2007. IGARSS 2007. IEEE International*, 2374-2377.

Quinlan, J. R., 1993. C4.5: Programs for Machine Learning. - Morgan Kaufmann Publisher, San Francisco, CA, USA.

Rodríguez-Cuenca B., J.A. Malpica, Alonso, M.C., 2012. Region growing segmentation of multispectral high resolution space images with open software, proc. of THE IEEE International Geoscience and Remote Sensing (IEEE Xplore), pp. 4311-4314.

Ruiz, L.A., Recio, J.A., Fernández-Sarría, A., Hermosilla, T., 2011. A feature extraction software tool for agricultural object-based image analysis. Computers and Electronics in Agriculture 76 (2), 284-296.

Shafer, G. 1976. A Mathematical Theory of Evidence. Princeton University Press.

Sutton, R.N., Hall, E.L., 1972. Texture Measures for Automatic Classification of Pulmonary Disease. - IEEE Transactions on Computers 21 (7): 667-676.

Van de Voorde, T., Van der Kwast, J., Engelen, G., Binard, M., Cornet, Y., Canters, F., 2009. Quantifying intra-urban morphology of the Greater Dublin area with spatial metrics derived from medium resolution remote sensing data. *Proceedings of the 7th International Urban Remote Sensing Conference, IEEE Geoscience and Remote Sensing Society*, *20-22 Mayo, Shanghai, China*, 6p.

Walter, V. 2004. Object-based classification of remote sensing data for change detection. *ISPRS Journal of Photogrammetry and Remote Sensing*, 58, (3-4), 225- 238.

Yoshida, H., Omae, M., 2005. An Approach for Analysis of Urban Morphology: Methods to Derive Morphological Properties of City Blocks by Using an Urban Landscape Model and Their Interpretations. - Computers, Environment and Urban Systems 29 (2): 223-247.

Yu, B., Liu, H., Wu, J., Hu, Y., Zhang, L., 2010. Automated Derivation of Urban Building Density Information Using Airborne LiDAR Data and Object-based Method. Landscape and Urban Planning 98 (3-4): 210-219.

Figure Index

Table Index

LIST OF OEEPE/EuroSDR OFFICIAL PUBLICATIONS

State – March 2013

1 Trombetti, C.: „Activité de la Commission A de l'OEEPE de 1960 à 1964" – Cunietti, M.: „Activité de la Commission B de l'OEEPE pendant la période septembre 1960 – janvier 1964" – Förstner, R.: „Rapport sur les travaux et les résultats de la Commission C de l'OEEPE (1960–1964)" – Neumaier, K.: „Rapport de la Commission E pour Lisbonne" – Weele, A. J. v. d.: „Report of Commission F." – Frankfurt a. M. 1964, 50 pages with 7 tables and 9 annexes.

2 Neumaier, K.: „Essais d'interprétation de »Bedford« et de »Waterbury«. Rapport commun établi par les Centres de la Commission E de l'OEEPE ayant participé aux tests" – „The Interpretation Tests of »Bedford« and »Waterbury«. Common Report Established by all Participating Centres of Commission E of OEEPE" – „Essais de restitution »Bloc Suisse«. Rapport commun établi par les Centres de la Commission E de l'OEEPE ayant participé aux tests" – „Test »Schweizer Block«. Joint Report of all Centres of Commission E of OEEPE." – Frankfurt a. M. 1966, 60 pages with 44 annexes.

3 Cunietti, M.: „Emploi des blocs de bandes pour la cartographie à grande échelle – Résultats des recherches expérimentales organisées par la Commission B de l'O.E.E.P.E. au cours de la période 1959–1966" – „Use of Strips Connected to Blocks for Large Scale Mapping – Results of Experimental Research Organized by Commission B of the O.E.E.P.E. from 1959 through 1966." – Frankfurt a. M. 1968, 157 pages with 50 figures and 24 tables.

4 Förstner, R.: „Sur la précision de mesures photogrammétriques de coordonnées en terrain montagneux. Rapport sur les résultats de l'essai de Reichenbach de la Commission C de l'OEEPE" – „The Accuracy of Photogrammetric Co-ordinate Measurements in Mountainous Terrain. Report on the Results of the Reichenbach Test Commission C of the OEEPE." – Frankfurt a. M. 1968, Part I: 145 pages with 9 figures; Part II: 23 pages with 65 tables.

5 Trombetti, C.: „Les recherches expérimentales exécutées sur de longues bandes par la Commission A de l'OEEPE." – Frankfurt a. M. 1972, 41 pages with 1 figure, 2 tables, 96 annexes and 19 plates.

6 Neumaier, K.: „Essai d'interprétation. Rapports des Centres de la Commission E de l'OEEPE." – Frankfurt a. M. 1972, 38 pages with 12 tables and 5 annexes.

7 Wiser, P.: „Etude expérimentale de l'aérotiangulation semi-analytique. Rapport sur l'essai »Gramastetten«." – Frankfurt a. M. 1972, 36 pages with 6 figures and 8 tables.

8 „Proceedings of the OEEPE Symposium on Experimental Research on Accuracy of Aerial Triangulation (Results of Oberschwaben Tests)“ Ackermann, F.: „On Statistical Investigation into the Accuracy of Aerial Triangulation. The Test Project Oberschwaben“ – „Recherches statistiques sur la précision de l'aérotriangulation. Le champ d'essai Oberschwaben“– Belzner, H.: „The Planning. Establishing and Flying of the Test Field Oberschwaben“ – Stark, E.: Testblock Oberschwaben, Programme I. Results of Strip Adjustments“ – Ackermann, F.: „Testblock Oberschwaben, Program I. Results of Block-Adjustment by Independent Models“ – Ebner, H.: Comparison of Different Methods of Block Adjustment“ – Wiser, P.: „Propositions pour le traitement des erreurs non-accidentelles“– Camps, F.: „Résultats obtenus dans le cadre du project Oberschwaben 2A“ – Cunietti, M.; Vanossi, A.: „Etude statistique expérimentale des erreurs d'enchaînement des photogrammes“– Kupfer, G.: „Image Geometry as Obtained from Rheidt Test Area Photography“ – Förstner, R.: „The Signal-Field of Baustetten. A Short Report“ – Visser, J.; Leberl, F.; Kure, J.: „OEEPE Oberschwaben Reseau Investigations“ – Bauer, H.: „Compensation of Systematic Errors by Analytical Block Adjustment with Common Image Deformation Parameters.“ – Frankfurt a. M. 1973, 350 pages with 119 figures, 68 tables and 1 annex.

9 Beck, W.: „The Production of Topographic Maps at 1 : 10,000 by Photogrammetric Methods. – With statistical evaluations, reproductions, style sheet and sample fragments by Landesvermessungsamt Baden-Württemberg Stuttgart.“ – Frankfurt a. M. 1976, 89 pages with 10 figures, 20 tables and 20 annexes.

10 „Résultats complémentaires de l'essai d'«Oberriet» of the Commission C de l'OEEPE – Further Results of the Photogrammetric Tests of «Oberriet» of the Commission C of the OEEPE“ Hárry, H.: „Mesure de points de terrain non signalisés dans le champ d'essai d'«Oberriet» – Measurements of Non-Signalized Points in the Test Field «Oberriet» (Abstract)“ – Stickler, A.; Waldhäusl, P.: „Restitution graphique des points et des lignes non signalisés et leur comparaison avec des résultats de mesures sur le terrain dans le champ d'essai d'«Oberriet» – Graphical Plotting of Non-Signalized Points and Lines, and Comparison with Terrestrial Surveys in the Test Field «Oberriet»“ – Förstner, R.: „Résultats complémentaires des transformations de coordonnées de l'essai d'«Oberriet» de la Commission C de l'OEEPE – Further Results from Co-ordinate Transformations of the Test «Oberriet» of Commission C of the OEEPE“ – Schürer, K.: „Comparaison des distances d'«Oberriet» – Comparison of Distances of «Oberriet» (Abstract).“ – Frankfurt a. M. 1975, 158 pages with 22 figures and 26 tables.

11 „25 années de l'OEEPE“

Verlaine, R.: „25 années d'activité de l'OEEPE“ – „25 Years of OEEPE (Summary)“ – Baarda, W.: „Mathematical Models.“ – Frankfurt a. M. 1979, 104 pages with 22 figures.

12 Spiess, E.: „Revision of 1 : 25,000 Topographic Maps by Photogrammetric Methods.“ – Frankfurt a. M. 1985, 228 pages with 102 figures and 30 tables.

13 Timmerman, J.; Roos, P. A.; Schürer, K.; Förstner, R.: On the Accuracy of Photogrammetric Measurements of Buildings – Report on the Results of the Test “Dordrecht”, Carried out by Commission C of the OEEPE. – Frankfurt a. M. 1982, 144 pages with 14 figures and 36 tables.

14 Thompson C. N.: Test of Digitising Methods. – Frankfurt a. M. 1984, 120 pages with 38 figures and 18 tables.

15 Jaakkola, M.; Brindöpke, W.; Kölbl, O.; Noukka, P.: Optimal Emulsions for Large-Scale Mapping – Test of “Steinwedel” – Commission C of the OEEPE 1981–84. – Frankfurt a. M. 1985, 102 pages with 53 figures.

16 Waldhäusl, P.: Results of the Vienna Test of OEEPE Commission C. – Kölbl, O.: Photogrammetric Versus Terrestrial Town Survey. – Frankfurt a. M. 1986, 57 pages with 16 figures, 10 tables and 7 annexes.

17 Commission E of the OEEPE: Influences of Reproduction Techniques on the Identification of Topographic Details on Orthophotomaps. – Frankfurt a. M. 1986, 138 pages with 51 figures, 25 tables and 6 appendices.

18 Förstner, W.: Final Report on the Joint Test on Gross Error Detection of OEEPE and ISP WG III/1. – Frankfurt a. M. 1986, 97 pages with 27 tables and 20 figures.

19 Dowman, I. J.; Ducher, G.: Spacelab Metric Camera Experiment – Test of Image Accuracy. – Frankfurt a. M. 1987, 112 pages with 13 figures, 25 tables and 7 appendices.

20 Eichhorn, G.: Summary of Replies to Questionnaire on Land Information Systems – Commission V – Land Information Systems. – Frankfurt a. M. 1988, 129 pages with 49 tables and 1 annex.

21 Kölbl, O.: Proceedings of the Workshop on Cadastral Renovation – Ecole polytechnique fédérale, Lausanne, 9–11 September, 1987. – Frankfurt a. M. 1988, 337 pages with figures, tables and appendices.

22 Rollin, J.; Dowman, I. J.: Map Compilation and Revision in Developing Areas – Test of Large Format Camera Imagery. – Frankfurt a. M. 1988, 35 pages with 3 figures, 9 tables and 3 appendices.

23 Drummond, J. (ed.): Automatic Digitizing – A Report Submitted by a Working Group of Commission D (Photogrammetry and Cartography). – Frankfurt a. M. 1990, 224 pages with 85 figures, 6 tables and 6 appendices.

24 Ahokas, E.; Jaakkola, J.; Sotkas, P.: Interpretability of SPOT data for General Mapping. – Frankfurt a. M. 1990, 120 pages with 11 figures, 7 tables and 10 appendices.

25 Ducher, G.: Test on Orthophoto and Stereo-Orthophoto Accuracy. – Frankfurt a. M. 1991, 227 pages with 16 figures and 44 tables.

26 Dowman, I. J. (ed.): Test of Triangulation of SPOT Data – Frankfurt a. M. 1991, 206 pages with 67 figures, 52 tables and 3 appendices.

27 Newby, P. R. T.; Thompson, C. N. (ed.): Proceedings of the ISPRS and OEEPE Joint Workshop on Updating Digital Data by Photogrammetric Methods. – Frankfurt a. M. 1992, 278 pages with 79 figures, 10 tables and 2 appendices.

28 Koen, L. A.; Kölbl, O. (ed.): Proceedings of the OEEPE-Workshop on Data Quality in Land Information Systems, Apeldoorn, Netherlands, 4–6 September 1991. – Frankfurt a. M. 1992, 243 pages with 62 figures, 14 tables and 2 appendices.

29 Burman, H.; Torlegård, K.: Empirical Results of GPS – Supported Block Triangulation. – Frankfurt a. M. 1994, 86 pages with 5 figures, 3 tables and 8 appendices.

30 Gray, S. (ed.): Updating of Complex Topographic Databases. – Frankfurt a. M. 1995, 133 pages with 2 figures and 12 appendices.

31 Jaakkola, J.; Sarjakoski, T.: Experimental Test on Digital Aerial Triangulation. – Frankfurt a. M. 1996, 155 pages with 24 figures, 7 tables and 2 appendices.

32 Dowman, I. J.: The OEEPE GEOSAR Test of Geocoding ERS-1 SAR Data. – Frankfurt a. M. 1996, 126 pages with 5 figures, 2 tables and 2 appendices.

33 Kölbl, O.: Proceedings of the OEEPE-Workshop on Application of Digital Photogrammetric Workstations. – Frankfurt a. M. 1996, 453 pages with numerous figures and tables.

34 Blau, E.; Boochs, F.; Schulz, B.-S.: Digital Landscape Model for Europe (DLME). – Frankfurt a. M. 1997, 72 pages with 21 figures, 9 tables, 4 diagrams and 15 appendices.

35 Fuchs, C.; Gülch, E.; Förstner, W.: OEEPE Survey on 3D-City Models.
Heipke, C.; Eder, K.: Performance of Tie-Point Extraction in Automatic Aerial Triangulation. – Frankfurt a. M. 1998, 185 pages with 42 figures, 27 tables and 15 appendices.

36 Kirby, R. P.: Revision Measurement of Large Scale Topographic Data.
Höhle, J.: Automatic Orientation of Aerial Images on Database Information.
Dequal, S.; Koen, L. A.; Rinaudo, F.: Comparison of National Guidelines for Technical and Cadastral Mapping in Europe (“Ferrara Test”) – Frankfurt a. M. 1999, 273 pages with 26 figures, 42 tables, 7 special contributions and 9 appendices.

37 Koelbl, O. (ed.): Proceedings of the OEEPE – Workshop on Automation in Digital Photogrammetric Production. – Frankfurt a. M. 1999, 475 pages with numerous figures and tables.

38 Gower, R.: Workshop on National Mapping Agencies and the Internet. Flotron, A.; Koelbl, O.: Precision Terrain Model for Civil Engineering. – Frankfurt a. M. 2000, 140 pages with numerous figures, tables and a CD.

39 Ruas, A.: Automatic Generalisation Project: Learning Process from Interactive Generalisation. – Frankfurt a. M. 2001, 98 pages with 43 figures, 46 tables and 1 appendix.

40 Torlegård, K.; Jonas, N.: OEEPE workshop on Airborne Laserscanning and Interferometric SAR for Detailed Digital Elevation Models. – Frankfurt a. M. 2001, CD: 299 pages with 132 figures, 26 tables, 5 presentations and 2 videos.

41 Radwan, M.; Onchaga, R.; Morales, J.: A Structural Approach to the Management and Optimization of Geoinformation Processes. – Frankfurt a. M. 2001, 174 pages with 74 figures, 63 tables and 1 CD.

42 Heipke, C.; Sester, M.; Willrich, F. (eds.): Joint OEEPE/ISPRS Workshop – From 2D to 3D – Establishment and maintenance of national core geospatial databases. Woodsford, P. (ed.): OEEPE Commission 5 Workshop: Use of XML/GML. – Frankfurt a. M. 2002, CD.

43 Heipke, C.; Jacobsen, K.; Wegmann, H.: Integrated Sensor Orientation – Test Report and Workshop Proceedings. – Frankfurt a. M. 2002, 302 pages with 215 figures, 139 tables and 2 appendices.

44 Holland, D.; Guilford, B.; Murray, K.: Topographic Mapping from High Resolution Space Sensors. – Frankfurt a. M. 2002, 155 pages with numerous figures, tables and 7 appendices.

45 Murray, K. (ed.): OEEPE Workshop on Next Generation Spatial Database – 2005. Altan, M. O.; Tastan, H. (eds.): OEEPE/ISPRS Joint Workshop on Spatial Data Quality Management. 2003, CD.

46 Heipke, C.; Kuittinen, R.; Nagel, G. (eds.): From OEEPE to EuroSDR: 50 years of European Spatial Data Research and beyond – Seminar of Honour. 2003, 103 pages and CD.

47 Woodsford, P.; Kraak, M.; Murray, K.; Chapman, D. (eds.): Visualisation and Rendering – Proceedings EuroSDR Commission 5 Workshop. 2003, CD.

48 Woodsford, P. (ed.): Ontologies & Schema Translation – 2004. Bray, C. (ed.): Positional Accuracy Improvement – 2004. Woodsford, P. (ed.): E-delivery – 2005. Workshops. 2005, CD.

49 Bray, C.; Rönsdorf, C. (eds.): Achieving Geometric Interoperability of Spatial Data, Workshop – 2005. Kolbe, T. H.; Gröger, G. (eds.): International Workshop on Next Generation 3D City Models – 2005. Woodsford, P. (ed.): Workshop on Feature/Object Data Models. 2006, CD.

50 Kaartinen, H.; Hyyppä J.: Evaluation of Building Extraction. Steinnocher, K.; Kressler, F.: Change Detection. Bellmann, A.; Hellwich, O.: Sensor and Data Fusion Contest: Information for Mapping from Airborne SAR and Optical Imagery (Phase I). Mayer, H.; Baltsavias, E.; Bacher, U.: Automated Extraction, Refinement, and Update of Road Databases from Imagery and Other Data. 2006, 280 pages.

51 Höhle, J.; Potuckova J.: The EuroSDR Test "Checking and Improving of Digital Terrain Models". Skaloud, J.: Reliability of Direct Georeferencing, Phase 1: An Overview of the Current Approaches and Possibilities. Legat, K.; Skaloud, J.; Schmidt, R.: Reliability of Direct Georeferencing, Phase 2: A Case Study on Practical Problems and Solutions. 2006, 184 pages.

52 Murray, K. (ed.): Proceedings of the International Workshop on Land and Marine Information Integration. 2007, CD.

53 Kaartinen, H.; Hyyppä, J.: Tree Extraction. 2008, 56 pages.

54 Patrucco, R.; Murray, K. (eds.): Production Partnership Management Workshop – 2007. Ismael Colomina, I.; Hernández, E. (eds.): International Calibration and Orientation Workshop, EuroCOW 2008. Heipke, C.; Sester, M. (eds.): Geosensor Networks Workshop. Kolbe, T. H. (ed.): Final Report on the EuroSDR CityGML Project. 2008, CD.

55 Cramer, M.: Digital Camera Calibration. 2009, 257 pages.

56 Champion, N.: Detection of Unregistered Buildings for Updating 2D Databases. Everaerts, J.: NEWPLATFORMS – Unconventional Platforms (Unmanned Aircraft Systems) for Remote Sensing. 2009, 98 pages.

57 Streilein, A.; Kellenberger, T. (eds.): Crowd Sourcing for Updating National Databases. Colomina, I.; Jan Skaloud, J.; Cramer, M. (eds.): International Calibration and Orientation Workshop EuroCOW 2010. Nebiker, S.; Bleisch, S.; Gülch, E.: Final Report on EuroSDR Project Virtual Globes. 2010, CD.

58 Stoter, J.: State-of-the-Art of Automated Generalisation in Commercial Software. Grenzdörffer, G.: Medium Format Cameras. 2010, 266 pages and CD.

59 Rönnholm, P.: Registration Quality – Towards Integration of Laser Scanning and Photogrammetry. Vanden Berghe, I.; Crompvoets, J.; de Vries, W.; Stoter, J.: Atlas of INSPIRE Implementation Methods. 2011, 292 pages and CD.

60 Höhle, J.; Potuckova M.: Assessment of the Qualityof Digital Terrain Models. 2011, 85 pages.

61 Fritsch, D.; Pfeifer, N.; Franzen, M. (eds.): High Density Image Matching for DSM Computation Workshop. 2012, CD.

62 Honkavaara, E.; Markelin, L.; Arbiol, R.; Martínez, L.: Radiometric Aspects of Digital Photogrammetric Images. Kaartinen, H.; Hyyppä, J.; Kukko, A.; Lehtomäki, M.; Jaakkola, A.; Vosselman, G.; Oude Elberink, S.; Rutzinger, M.; Pu, S.; Vaaja, M.: Mobile Mapping - Road Environment Mapping using Mobile Laser Scanning. 2013, 95 pages.

63 Fritsch, D.; Pfeifer, N.; Franzen, M. (eds.): 2nd High Density Image Matching for DSM Computation Workshop. 2013, CD.

The publications can be ordered using the electronic order form of the EuroSDR website www.eurosdr.net